A Serial Multiplex Immunogold Labeling Method for Identifying Peptidergic Neurons in Connectomes

Réza Shahidi[1], Elizabeth A. Williams[1], Markus Conzelmann[1], Albina Asadulina[1], Csaba Verasztó[1], Sanja Jasek[1], Luis A. Bezares-Calderón[1] and Gáspár Jékely[1*]

[1]Max-Planck-Institute for Developmental Biology, Spemannstraße. 35, Tübingen D- 72076, Germany

[*]Corresponding author
Email: gaspar.jekely@tuebingen.mpg.de

Competing interests: The authors declare that no competing interests exist.

ABSTRACT

Electron microscopy-based connectomics aims to comprehensively map synaptic connections in neural tissue. However, current approaches are limited in their capacity to directly assign molecular identities to neurons. Here, we use serial multiplex immunogold labeling (siGOLD) and serial-section transmission electron microscopy (ssTEM) to identify multiple peptidergic neurons in a connectome. The high immunogenicity of neuropeptides and their broad distribution along axons, allowed us to identify distinct neurons by immunolabeling small subsets of sections within larger series. We demonstrate the scalability of siGOLD by using 11 neuropeptide antibodies on a full-body larval ssTEM dataset of the annelid *Platynereis*. We also reconstruct a peptidergic circuitry comprising the sensory nuchal organs, found by siGOLD to express pigment-dispersing factor, a circadian neuropeptide. Our approach enables the direct overlaying of chemical neuromodulatory maps onto synaptic connectomic maps in the study of nervous systems.

INTRODUCTION

A comprehensive understanding of nervous system function requires knowledge of not only precise neuronal connectivity but also of the unique combinations of molecules expressed by each neuron. Connectomics using serial-sectioning electron microscopy (EM) aims to map the synapse-level connectivity of entire neural circuits (Morgan and Lichtman, 2013). However, wiring diagrams provide an incomplete picture of the nervous system, since they lack information about the molecular nature of neurons.

One important class of molecules are neuromodulators, including monoamines and neuropeptides, that actively shape the output of circuits by modifying synaptic function and neuron excitability (Bargmann, 2012; Bargmann and Marder, 2013; Bucher and Marder, 2013; Marder, 2012). The direct mapping of specific neuromodulators to their source cells in synapse-level anatomical maps would help to integrate connectomic and neuromodulatory perspectives, thereby enriching our understanding of circuit function.

Several approaches have been developed to assign molecular identities to neurons on EM sections. Genetically encoded tags with enzymatic activity, such as miniSOG and APEX probes, allow the resolution of cells or subcellular structures by EM following incubation with a substrate that is

converted to electron-dense deposits (Martell et al., 2012; Shu et al., 2011). Fixation resistant protein tags compatible with EM procedures and observable by correlative light and electron microscopy (CLEM) or directly by immunogold labeling (immunoEM), such as the smGFPs (Viswanathan et al., 2015), have also been developed. In CLEM, fluorescently labeled neurons or organelles can be imaged live prior to fixation, sectioning, and EM imaging of the specimen. Fiducial markers allow the correlation of cellular structures in the IF and EM images (Colombelli et al., 2008; Maco et al., 2013; Maco et al., 2014; Urwyler et al., 2015). However, the neuron-specific probes employed by these technologies must be expressed using transgenesis, limiting their use to one or a few markers, such as in the "two-tag" labeling approach (Lin et al., 2015).

An alternative approach to assigning molecular identities to neurons is the use of endogenous targets in fixed specimen, as in array tomography, a method employing sequential immunofluorescence (IF) with several different antibodies on large series of sections (Collman et al., 2015; Micheva and Smith, 2007). IF imaging can be combined with scanning EM imaging of selected sections to resolve ultrastructural detail. The sequentially acquired IF and EM images can be registered, allowing for correlative analysis of images of different modalities (Collman et al., 2015). However, the sequential IF procedure compromises the membrane contrast in EM, preventing the reliable tracing of fine processes across series of sections (Collman et al., 2015). Array tomography also relies on embedding the specimen in porous, hydrophilic acrylic resins to allow optimal immunolabeling. For large-scale serial sectioning projects, epoxy resins, such as Epon, are favored due to their higher stability during sectioning and imaging and the optimal ultrastructural preservation they provide (Bock et al., 2011; Briggman et al., 2011; Bumbarger et al., 2013; Ohyama et al., 2015; Randel et al., 2015; White et al., 1986). Unfortunately, the Epon-embedding procedure, including osmium-fixation and resin polymerization at 60 °C, compromises the immunogenicity of many endogenous targets (Brorson, 1998; Brorson and Reinholt, 2008; De Paul et al., 2012). Current immunolabeling approaches therefore sacrifice the mechanical stability and ultrastructural contrast of the sample for optimal immunolabeling.

One exception is short amidated neuropeptide antigens, that show good immunopreservation in epoxy-embedded samples (Hamanaka et al., 2010; Koizumi et al., 1989; Merighi et al., 1992; Yasuyama and Meinertzhagen, 2010). Such antigens represent promising targets in an attempt to combine connectomics on Epon-embedded samples and immunogold labeling for specific neuromodulators. Neuropeptides are often chemically modified, including C-terminal amidation (Eipper et al., 1992), which confers stability and high immunogenicity to even very short peptides (Conzelmann and Jékely, 2012). Furthermore, neuropeptides show neuron-type specific expression and are distributed throughout the axon of peptidergic neurons (Wong et al., 2012; Zupanc, 1996), representing useful markers for neuron-type identification.

Here, we introduce serial-multiplex immunogold (siGOLD), a method for immunolabeling connectomes. siGOLD involves immunogold labeling of small subsets of sections from large series with different neuron-type-specific neuropeptide antibodies. The molecularly identified neurons and their synaptic partners are then reconstructed from the entire aligned series using standard EM-based connectomics.

We established siGOLD using larval stages of *Platynereis dumerilii*, a marine annelid that has recently emerged as a powerful model for circuit neuroscience, genetics, and whole-body connectomics (Backfisch et al., 2013; Bannister et al., 2014; Gühmann et al., 2015; Randel et al., 2014; Randel et al., 2015; Tosches et al., 2014; Veedin-Rajan et al., 2013; Zantke et al., 2014). We identified several amidated neuropeptide epitopes that showed long-term immunopreservation in Epon-embedded samples, allowing us to simultaneously obtain high ultrastructural detail and specific immunogold signal. Using siGOLD with 11 distinct antibodies on the same specimen, we identified several neuropeptide-containing neuron profiles in a whole-body *Platynereis* larval serial

EM dataset (Randel et al., 2015). Furthermore, taking advantage of the whole-body series, we fully reconstructed several peptidergic neurons identified by siGOLD in the *Platynereis* larva. We also identified and reconstructed the postsynaptic partners of selected peptidergic neurons, focusing on the nuchal organs, paired, putatively chemosensory organs with high structural complexity and variability among the annelids (Purschke, 1997; Purschke, 2005; Purschke et al., 1997; Schlötzer-Schrehardt, 1987). Our work demonstrates that siGOLD can be used in large serial EM datasets to assign molecular identities to multiple neurons using different markers and to fully reconstruct and analyze the synaptic connectivity of these neurons at EM resolution.

RESULTS

Multiplex neuron identification with siGOLD on serial sections

In order to selectively label individual neurons in large-scale serial EM datasets, we established an immunoEM procedure to label ultrathin sections with neuronal cell-type specific antibodies. We reasoned that immunoEM performed on only a few layers from a large series of sections could identify neuron profiles that contain the antigen (Figure 1A). We first performed immunoEM on 40-nm serial sections from the ventral nerve cord (VNC) of a 72 hours post-fertilization (hpf) *Platynereis* larva (specimen HT9-5, Figure 1B, C). For specimen preparation, we used a conventional serial TEM protocol including high-pressure freezing, fixation with a freeze substitution medium containing 2% osmium tetroxide and 0.5% uranyl acetate, and embedding in Epon. We also developed a procedure for the safe handling of several grids in parallel during the immunostaining and contrasting procedure. We optimized the immunolabeling protocol to achieve high specificity for immunoEM and high ultrastructural detail. In our protocol, we use secondary antibodies coupled to ultra small gold particles and a silver-enhancement procedure. We also fine-tuned the contrast-staining protocol to optimize contrast for both gold labeling and ultrastructural detail.

In preliminary tests, we found strong and localized labeling in neurites using 11 different polyclonal antibodies generated against short amidated neuropeptides of *Platynereis* (Table 1).

To test the specificity and reproducibility of immunoEM with the 11 neuropeptide-antibodies, we collected two sets of transverse serial sections from the 1st trunk segment of the HT9-5 specimen. 4 to 18 consecutive serial sections were collected on each EM grid for immunoEM. For each antibody, we stained two grids separated by a serial distance of approximately 50 sections (Figure 1C). We imaged the VNC region in each section at high resolution (2.22 nm/pixel) followed by stitching and alignment of the images. We found strong and localized labeling in only a small subset of neurites for each antibody (Figure 2A, Shahidi et al. 2015). In consecutive sections, the same neurite was often strongly labeled with the same antibody (Figure 2A, FVa, layers 1-5). In sections collected on different grids that were labeled with different antibodies, we found distinct patterns of neurite-specific labeling (Figure 2B, C). In many sections, we could observe dense core vesicles (DCVs) in the cytoplasm of the gold-labeled neurites, indicative of the peptidergic nature of these cells (Figure 2A-F, Shahidi et al. 2015). In high-resolution (0.22 nm/pixel) images we could observe gold labeling associated with DCVs (Figure 2D-F), suggesting that our immunoEM procedure labeled mature neuropeptides residing inside these vesicles. Several ultra-small gold particles were not enlarged during the silver-enhancement procedure but were also associated with DCVs (Figure 2D-F).

Next, we comprehensively scored the distribution of gold particles in the VNC series (Figure 3). We selected all neurites that were labeled with two or more gold particles in any of the immunoEM

sections and traced these neurites across all sections. We also selected 50 control neurites along a coronal transect spanning the VNC and traced these across all sections (Figure 3A). We then counted all gold particles in each traced neurite and tabulated the results (Figure 3 – source data 1). The gold particles were also summed for each antibody to show a concise summary of all gold labels (Figure 3B and D). Since not all ultra-small gold particles were enhanced during silver-enhancement (Figure 2D-F) and non-enhanced particles are not visible on the lower-resolution images we used for scoring, the gold counts likely underestimate the intensity of gold labeling.
Our quantifications revealed a high neurite-specificity of immunogold labeling with all 11 neuropeptide antibodies (Figure 3). In sections where we omitted the primary antibody, we did not see any gold labeling in any of the traced neurites (Figure 3B). The VNC in our sample contained approximately 1600 neurite cross-sections and the majority of these showed no gold labeling. However, for each antibody we could identify a small number of neurites that consistently showed strong labeling across different sections (Figure 3, Figure 3 – source data 1). The pattern of the labeled neurites in the VNC showed bilateral symmetry, supporting the labeling of specific peptidergic neuron populations on the left and right sides of the body. Most neurites that were labeled on one grid were also strongly labeled on their grid pair with the same antibody separated by approximately 50 sections. There were some exceptions, for example neurite n5 that was labeled strongly with the FVamide antibody in layers 18-23 but not in layers 69-74 (Figure 3 – source data 1). To determine whether the lack of labeling was due to the lack of DCVs in these sections, we scored the number of DCVs across all sections for selected neurites (Figure 3 – figure supplement 1). We found that DCVs were non-uniformly distributed in the neurites and some sections completely lacked DCVs. Importantly, we only detected gold labeling on sections that contained DCVs in the respective neurite (Figure 3 – source data 1).
siGOLD also allowed us to detect the coexpression of some neuropeptides in the same neurons. For example, we found coexpression of FVa and PDF neuropeptides in a subset of the neurites labeled by these two antibodies (Figure 3D). Some antibodies showed extensive overlap in labeling, including the FMRFa, luqin and RYa antibodies.
To test whether the antibodies specifically recognize the neuropeptides used for immunization, we performed morpholino-mediated knockdown experiments of proneuropeptide expression. The specificity of the MIP antibody was demonstrated previously (Williams et al., 2015). We performed microinjections with 10 different translation-blocking morpholinos, one targeting each remaining proneuropeptide. We then performed triple IF in whole-mount 72 hpf larval samples using an acetylated tubulin antibody, a rat FVa antibody, and the respective rabbit neuropeptide antibodies. The acetylated tubulin antibody allowed us to exclude developmental abnormalities caused by morpholino injection. The rat FVa antibody provided a further control to exclude that morpholino injection affected proneuropeptide processing in general. For eight out of 10 antibodies (FVa, FMRFa, ATO, FVRIa, PDF, RGWa, PENK, LEUC), morpholino injection strongly reduced IF signal with the respective antibody (Figure 4 – figure supplement 1). For the FMRFa antibody, we did not detect staining in the VNC following morpholino injection, but we could still detect staining in the head. The FMRFa antibody therefore likely recognizes other antigens, such as other RFa peptides in the head (Conzelmann et al., 2013b). For the RYa and LUQ antibodies, we did not see a reduction in staining intensity in the VNC following morpholino injection. These two antibodies may cross-react with other R[Y|F]amide peptides as suggested by the labeling of an overlapping set of neurites with the FMRFa, LUQ, and RYa antibodies (Figure 3). Without knowing the exact antigen specificity for these antibodies, we can nevertheless use them as specific markers of R[Y|F]amidergic neurons.

Comparison of siGOLD labeling to whole-mount immunofluorescence

siGOLD labeling of consecutive sections with 11 antibodies revealed the arrangement of several peptidergic neurites in the VNC (Figure 3). To test if this spatial arrangement is consistent between siGOLD and IF labeling of whole specimens we analyzed the labeling with all 11 antibodies in whole-mount *Platynereis* 72 hpf larval samples. All antibodies labeled subsets of longitudinal axons spanning the entire length of the VNC and occurring in different mediolateral positions (Figure 4). To display the spatial relationships of 11 distinct IF labels, we employed image registration to a reference template of whole-body confocal scans. High-accuracy image registration of different specimens is possible in *Platynereis*, due to the stereotypic anatomy and neuronal connectivity of the larvae (Asadulina et al., 2012; Randel et al., 2015; Tomer et al., 2010). For optimal VNC registration, we generated an unbiased average whole-body reference template based on the non-rigid registration of the acetylated tubulin IF signal from 36 specimens. We aligned whole-body confocal scans of IF specimens to this reference using non-rigid image registration (Figure 5A, B; Video 1). We then took virtual cross sections from this registered dataset to analyze the spatial relationships of distinct peptidergic axons (Figure 5C-E). The arrangement of peptidergic axons in the VNC reconstructed by IF and image registration was similar to that of the VNC reconstructed by siGOLD (Figure 5F-H). To allow a more direct comparison of the spatial relationship of peptidergic axons, we performed double IF with each of the RGWa, PDF, and LEUC antibodies generated in rabbits in combination with a FVa antibody generated in rats. The spatial relationships of the neurites labeled with the RGWa, PDF, and LEUC antibodies relative to six prominent FVa neurites was very similar between IF and siGOLD (Figure 5I, J). We could also detect the coexpression of FVa and PDF in some axons, both by double-IF and siGOLD. The high specificity of immunoEM, the reproducibility of labeling across sections, and the spatial correspondence of the labels between siGOLD and whole-mount IF indicate that we could accurately identify different peptidergic neurites in a serial EM dataset.

Application of siGOLD to a whole-body connectome dataset

Next, we tested siGOLD on a whole-body EM series of 5056 sections encompassing an entire 72 hpf *Platynereis* larva (specimen HT9-4)(Randel et al., 2015). During sectioning of this larva, we set aside series of 1 to 6 sections for later immunoEM (Figure 6 – source data 1).
In the full-body series, we used the 11 rabbit antibodies (Table 1) to label a total of 154 sections (3% of all sections) distributed along the length of the larva (Figure 6A). We used at least two grids for each antibody, separated by up to 1,000 sections. Gold labeling in a whole-body context allowed us to identify several strongly labeled neurite profiles throughout the body. It is worth noting that sections were successfully gold labeled up to 3 years after sectioning the specimen, demonstrating the long-term stability of neuropeptide antigens in Epon sections.
We identified and traced 83 neurons (67 of them with a soma; Figure 6B; Video 2) with different peptidergic identities. We mapped the distribution of peptidergic axons crossing a section in the 1st trunk segment in a position comparable to that of HT9-5 and found similar patterns across both siGOLD-labeled larvae and the IF samples (Figure 7A, B; compare to Figure 5). For selected neurons, we quantified the number of gold particles in every immunolabeled section in HT9-4 (Figure 8, Figure 9). These counts again demonstrated that we could repeatedly label the same neurons in different sections, often spaced several hundred sections apart.
The reconstruction of several neurons in the whole-body serial EM dataset allowed us to further test the specificity of the immunogold labels by comparing the morphology and position of reconstructed neurons to neurons that were identified by whole-body IF. We found comparable

cellular morphologies and positions for six FVa, several PDF (Figure 8), two RGWa, and four MIP neurons (Figure 9) between siGOLD and IF. This close anatomical correspondence further supports the specificity of siGOLD and demonstrates that the method can be used to unambiguously tag fully reconstructed neurons in serial EM.

Connectome reconstruction of a siGOLD-labeled peptidergic circuit

The whole-body serial EM dataset combined with siGOLD labeling allows the reconstruction of circuits of neurons with specific peptidergic identities. To demonstrate this, we focused on the nuchal organs in the *Platynereis* larval head as an example. The nuchal organ is a paired putative chemosensory organ in the annelid head with sensory neurons projecting a sensory dendrite into an olfactory pit. The olfactory pit is covered by cuticle and is associated with a patch of motile cilia (Figure 10A-C; Video 3)(Purschke, 2005). We found that several sensory neurons of the nuchal organs (SN^{nuch}) were strongly labeled by the PDF antibody in three different PDF-labeled sections in the head (Figure 6A; Table 2). Of the 35 SN^{nuch} cells we identified, 15 were labeled with the PDF antibody, with some of the neurons showing strong gold labeling in multiple sections (Table 2). This is consistent with the labeling of the nuchal organ with the PDF antibody in IF (Figure 8G). We traced all SN^{nuch} neurons and identified their direct postsynaptic targets. We found that the most strongly connected neurons, receiving up to 22 synapses from SN^{nuch} cells, were two pairs of interneurons (IN^{arc}) with a unique biramous morphology and contralaterally projecting axons (Figure 10D-F; Figure 10 – figure supplement 1; Video 4). Two of the IN^{arc} neurons were previously shown to be postsynaptic to the photoreceptor cells of the larval eyespots and have connections to the ventral motorneurons (Randel et al., 2015). This represents a potential functional path linking the nuchal organs to the locomotor apparatus. We also identified several other neurons that received a few synapses from the SN^{nuch} cells, including two interneurons (IN^{RGWr1}, IN^{RGWl1}) that were identified by siGOLD labeling to express the RGWa neuropeptide (Figure 9A, B). Additionally, 87 neurons received only one synapse from one of the SN^{nuch} cells (Figure 10 – figure supplement 2). The strong connectivity of the IN^{arc} cells to the nuchal organ relative to these other neurons suggests that the IN^{arc} cells represent the functionally relevant targets in the circuit. Mapping the position of presynaptic sites of SN^{nuch} cells revealed that these cells form synapses bilaterally (Figure 10 H, I). This is in contrast to the adult eye photoreceptor cells that only form ipsilateral synapses (Figure 10 H, I)(Randel et al., 2014).
To characterize the synapses of the PDF-positive SN^{nuch} cells in more detail, we examined several synapses in high-resolution (2.22 nm/pixel) images (Randel et al., 2015). We found that SN^{nuch} presynaptic sites contained only DCVs (Figure 10J, K). These synapses could be clearly distinguished from classical neurotransmitter synapses (Figure 10 L)(Randel et al., 2014) based on the larger size of the synaptic vesicles (mean diameter=63 nm, st.dev.=8.4, n=100 vesicles) and the electrondense core of the vesicles (Figure 10J, K). Furthermore, mapping classical neurotransmitter markers by *in situ* hybridization did not reveal the presence of any classical neurotransmitters in the nuchal organ region (Randel et al., 2014). Although we did not directly immunogold label any of the SN^{nuch} synapses, these observations suggest that the SN^{nuch} neurons signal to their target interneurons by PDF-containing vesicles concentrated at peptidergic synapses.

DISCUSSION

In this paper we introduced siGOLD, a method to molecularly identify specific neurons in large serial EM datasets based on the immunogold labeling of subsets of sections followed by serial reconstruction of the tagged neurons. Due to the sparse labeling of a few sections across many, siGOLD allows the use of several different antibody labels, each at different sections, within a single dataset. siGOLD relies on continuous series of sections of sufficient quality that allow the tracing of neurites in order to reconstruct the morphologies of labeled neurons.

Since siGOLD requires the sparse labeling of small subsets of sections, it is ideally used with markers that broadly label a neuron's morphology. We established siGOLD using neuropeptide antibodies for two reasons. First, neuropeptides are distributed along the entire length of axons, due to their active circulation throughout the axon (Wong et al., 2012). Second, neuropeptide antigens have unique properties, including their small size, high abundance, concentration in DCVs, and frequent C-terminal amidation, a modification that confers increased stability and immunogenicity to mature neuropeptides (Conzelmann and Jékely, 2012; Eipper et al., 1992). In agreement with the extreme stability of neuropeptide immunoreactivity, we could perform immunoEM of 'set-aside' layers using neuropeptide antibodies years after sectioning and the acquisition of the complete image series had been completed.

We did not test other antibodies, but several generally used antibody markers, including antibodies against neurotransmitters, transporters, or enzymes (Collman et al., 2015), could in principle be suitable for neuron identification using siGOLD. We established siGOLD on Epon-embedded samples that allowed robust sectioning of thousands of sections and provided high ultrastructural detail. Since Epon-embedding is known to compromise the immunogenicity of some antigens (Brorson, 1998; Brorson and Reinholt, 2008; De Paul et al., 2012), labeling for such antigens may require the use of alternative embedding resins such as Lowicryl HM-20 that provides excellent ultrastructural contrast and is compatible with many antibodies (Collman et al., 2015).

siGOLD is compatible with conventional TEM using sections collected on slotted, plastic-coated nickel grids (Skepper and Powell, 2008). It is also compatible with sectioning methods that collect long ribbons of sections on a glass slide (Blumer et al., 2002) or the high-throughput automatic tape-collecting ultramicrotome (ATUM) method (Hayworth et al., 2014). However, siGOLD is not compatible with sectioning procedures that destroy the sections, such as focused ion beam (FIB) SEM (Reyntjens and Puers, 2001) or the serial block-face method (Denk and Horstmann, 2004).

The siGOLD method differs from conjugate light-electron array tomography (Collman et al., 2015) and CLEM in several aspects. Array tomography was developed to provide detailed molecular profiling of individual synapses, and uses repeated immunolabeling of every section. siGOLD does not rely on the staining of every section with multiple markers, but rather the staining of sparsely distributed sections with one marker each. The aim of siGOLD is to assign molecular tags to several different neurons and to trace them through many layers. Array tomography and CLEM involves the registration of separately acquired IF and EM images, and the relocation of the sample between the different imaging setups can be challenging and time consuming (Timmermans and Otto, 2015). In contrast, siGOLD relies on the direct immunoEM labeling of sections and no registration step is needed. With siGOLD we enjoy the full resolving power of the electron microscope, and in this study we could also identify individual DCVs that carry strong immunogold signal in the neurite profile of specific peptidergic neurons.

One shortcoming of the immunoEM approach is that sections cannot be relabeled after they have been contrasted and exposed to the electron beam. However, given that in siGOLD only a subset of the sections is processed for immunoEM, it is possible to use an arbitrarily large number of antibodies at different sections from a series that encompasses a large volume of tissue, allowing the multiplex identification of neuron types.

We demonstrated that siGOLD can be used to molecularly identify neurons in large serial EM datasets, in conjunction with the reconstruction of the synaptic connectivity of these neurons. We reconstructed the sensory neurons of the nuchal organs and their postsynaptic partners, representing a candidate chemotactic circuit in the *Platynereis* larval head. siGOLD labeling revealed that the sensory neurons express the PDF neuropeptide. The presence of DCVs and lack of clusters of clear vesicles at presynaptic sites in these neurons suggest the presence of peptidergic transmission to the target interneurons.

The bilateral projection of the nuchal organ sensory neurons is similar to that seen for olfactory receptor neurons in *Drosophila*. These neurons form bilateral projections, and the lateralization of odor processing is achieved by an asymmetry in neurotransmitter release (Gaudry et al., 2013). The nuchal organ circuit may use a similar computational strategy, and this is likely different from the processing of visual information (Randel et al., 2014; Randel et al., 2015). The molecular information obtained by siGOLD provides a useful entry point to the genetic investigation of this putative chemotactic circuit in *Platynereis*.

The mapping of peptidergic neurons by siGOLD, together with the recent identification of several neuropeptide receptors in *Platynereis* (Bauknecht and Jékely, 2015), open up the possibility of a cellular-level analysis of peptidergic neurotransmission in diverse circuits in *Platynereis*. In total, we have identified 83 different peptidergic neurons out of approximately 2000 total in the *Platynereis* whole-body dataset. Further connectome tracing in these data will provide a rich source of information about specific peptidergic circuit motifs in this animal.

The siGOLD approach and the use of neuropeptide antibodies could also be adapted to enrich connectome data with molecular information in other organisms. In *Platynereis*, as well as vertebrates, *C. elegans*, and *Drosophila*, the majority of mature neuropeptides are amidated (Jékely, 2013; Mirabeau and Joly, 2013), and several antibodies are available (e.g., (Johard et al., 2008; Nässel, 1993)) or could readily be generated. Some neuropeptide antibodies have already been shown to work with immunoEM. For example, PDF neuropeptide-containing neurons were identified in the *Drosophila* brain by immunoEM and their local synaptic inputs were reconstructed from a series of sections (Yasuyama and Meinertzhagen, 2010). This and other antibodies could be used for siGOLD labeling in larger-scale connectome projects in *Drosophila*. Similar protocols and reagents could also be established for other organisms. siGOLD could also be adapted to organisms where transgenic tools to deliver EM-compatible markers are not available. In such organisms, the use of cross-species antibodies (Conzelmann and Jékely, 2012; Nässel, 1993) is a promising approach that would also allow the comparison of specific peptidergic neurons and their circuits across species.

The direct overlaying of chemical neuromodulatory maps onto synaptic connectomic maps by siGOLD opens up new possibilities for the study of nervous systems.

MATERIALS AND METHODS

Transmission electron microscopy

Fixation and embedding was carried out on 72 hpf *Platynereis* larvae (HT9-4 and HT9-5) as described previously (Conzelmann et al., 2013a). 40 nm serial sections were cut on a Reichert Jung Ultracut E microtome using a 45º DiATOME Diamond knife. The sections were collected on single-slotted copper grids (NOTCH-NUM 2_1 mm, Science Service, Munich) with Formvar support film. For the HT9-5 serial sections, the samples were collected on single-slotted nickel grids coated with Formvar support film. The ribbons of sections were picked up from underneath

and on the under-side (the notch side) of the grids. This method allowed the section ribbons to stay afloat and stretch while being dried in the oven, eliminating most wrinkles from the sections. The section statistics for the HT9-4 specimen (or NAOMI) were previously described (Randel et al., 2015) and an updated table with the immunoEM information is shown in Figure 6 – source data 1. For HT9-5, 200 sections were cut from the VNC (first segment) and imaged for tracing, segmentation and analysis.

Grid handling

To meet the demand for consistent section processing in large-scale serial reconstruction projects, we have developed an effective method of grid handling based on a method first described in (Rowley and Moran, 1975). The following method has proven safe for contrast staining, immunolabeling, and carbon coating. It stabilizes the grids during the staining procedures and saves time by eliminating the need for one-by-one grid manipulation.
A 6x12 hole microwell mini tray plate (NUNC™ Brand MicroWell® Mini Trays) was cut into two 3x12 hole plate strips. Holes were drilled through each of the plate's micro-cups using a fine drill to later allow the plastic support film to dry evenly on both sides. Plates were rinsed with 75% ethanol, followed by distilled water, then sonicated to eliminate dust and burr particles. This procedure produced two lightweight plates similar to that described in (Rowley and Moran, 1975) with the additional benefit of 'raised', separated walls. This approach prevents cross-contamination by diffusion of solutions during the staining and labeling procedures. A strip of Formvar support film was used to coat the microwell mini plate on the topside of the plate. A small water droplet (10 µl) was placed on each hole of the plate on the support film using a filtered syringe. A grid containing previously cut sections was placed (sections facing up) on each droplet and dried in the 50ºC oven until the grids and the plastic support film had fused. Grids were then ready for immunolabeling and contrast staining by inverting and matching to the micro-cups of a full mini tray with desired solutions (Figure 1A – Mini tray).

Contrasting

Dried sections were contrast stained with drops of 2% aqueous uranyl acetate for 6 min. Grids were washed by gently lowering the entire plate into a clean glass beaker of filtered distilled water. Excess water was wicked away with filter paper and the grids were dried at 50 ºC for 1-2 min. Next, the grids were stained with drops of Sato's triple lead stain (Hanaichi et al., 1986) for 4 min. Grids were washed and dried as described above and dried at 50 ºC for 1 min. Grids were then carbon coated before being imaged with a FEI TECNAI Spirit electron microscope.

Immunogold silver-enhancement method

For immunoEM, we have eliminated the etching step prior to primary antibody incubation. We have observed that the treatment with the etching solution destroys ultrastructural integrity. In our technique, the use of sheep serum and bovine serum albumin mixed with Tween-20 at pH of 7.9 greatly enhanced the immunogold signal.
The following protocol was performed over a one-day period and is an optimized version of a protocol by Stierhof (Stierhof et al., 1991) for Epon-embedded sections. All incubations up to the silver enhancement point were done in the TBST-BGN (Tris buffer saline with Tween-20, BSA, Fish Gelatin and Normal Sheep Serum, pH 7.9; see section below on preparing the buffer). First, sections were blocked with TBST-BGN for 10 minutes; blocked sections were then incubated with

primary antibody (1:25 dilution) in TBST-BGN for 2 hours. Grids were washed twice with TBST-BGN for 5 minutes, and then incubated with secondary goat anti-rabbit IgG antibody with gold conjugates (AURION Ultra Small Immunogold Reagents; size 0.8 nm) at 1:50 dilution for 1 hour. Grids were then washed with TBST-BGN twice for 5 minutes, then washed twice with filtered distilled water for 5 minutes, followed by fixation with 1% glutaraldehyde in filtered distilled water for 5 min. Sections were washed in filtered distilled water twice for 5 min. Silver enhancement was applied with Aurion silver-enhancement kit for up to 47 minutes. The time interval of silver enhancement was dependent on temperature and concentration of the silver-enhancement solution. Gold size growth was approximately 15-20 nm within this time interval, a size appropriate for observation of gold particles in EM. Silver enhancement was stopped with three 3-minute washes in filtered distilled water. Excess water was gently wicked from the back of the plate and individual holes with wedges of Whatman filter paper. Grids were dried in a 50 ºC oven and then contrasted (see above).

Preparation of blocking and wash buffer solution

Buffer concentration and consistency is very important in immunological reactions. We compared many protocols to achieve the best buffer for our experiments. We found that a saline buffer with Tris, Tween, bovine serum albumin (BSA), fish Gelatin, and normal serum (TBST-BGN), worked well. Our solutions were always freshly prepared on the day of the experiment. To prepare the buffer for immunoEM, three separate solutions were made: (1) 0.61 g Trizma, 0.90 g NaCl, and 70 ml of distilled water, (2) 1.0 g of BSA, 1.5 ml normal sheep serum, 500 µl Tween-20, and 20 ml distilled water, and (3) 0.01g of fish Gelatin and 10 ml of distilled water. Solution 3 was heated to dissolve and then cooled before being added to solution 1 and 2. Finally, solutions 1-3 were combined and gently mixed. The buffer solution was then adjusted to pH of 7.9 using 1 M HCl and syringe filtered with a 0.45 µm filter.

Imaging and post-processing

Image acquisition of TEM serial sections was performed on a FEI TECNAI Spirit transmission electron microscope equipped with an UltraScan 4000 4X4k digital camera using the image acquisition software Digital Micrograph (Gatan Software Team Inc., Pleasanton) and SerialEM (Mastronarde, 2005). The images for the HT9-4 and HT9-5 samples were scanned at a pixel resolution of 5.71 nm/pixel and 2.22 nm/pixel respectively. Image stitching and alignment were accomplished using TrakEM2 (Cardona et al., 2010; Cardona et al., 2012). All structures were segmented manually as area-lists, and exported into 3Dviewer and Blender as previously described (Asadulina et al., 2015). Tracing and annotation of the connectome were performed with CATMAID, a collaborative annotation toolkit for large-scale image data (Saalfeld et al., 2009; Schneider-Mizell et al., 2015).

IF and image registration

Antibodies were generated by immunizing rats or rabbits with synthetic, amidated peptides. Some of the antibodies were used in previous studies (Conzelmann and Jékely, 2012; Conzelmann et al., 2011; Conzelmann et al., 2013a; Jékely et al., 2008). All peptides contained an N-term Cys that was used for coupling. Antibodies were affinity purified from sera as previously described (Conzelmann and Jékely, 2012). Immunostainings were carried out as previously described (Conzelmann and Jékely, 2012). For triple IF, we used secondary antibodies coupled to three different fluorophores

(FVa rat, AF488 secondary antibody rat; other neuropeptide rabbit, AF647 secondary antibody rabbit; acetylated-tubulin mouse, high-fidelity AF555 secondary antibody mouse).
For image registration, an average full-body acetylated tubulin reference template was generated for 72 hpf *Platynereis* using a modification of a previously described method (Figure5 – source data 1) (Asadulina et al., 2012). We used full-body scans of 36 larvae generated on a Zeiss LSM 780 confocal microscope with ZenBlue software. All stacks were oriented and their centers of mass were aligned. Stacks were averaged and all stacks were aligned to this first average template using affine transformation. The 24 registered stacks most similar to the first average (as determined by an iteration metric) were then used to create an affine-transformed average. All original oriented stacks were then aligned to the affine-transformed average using affine and deformable transformation. The 24 registered stacks most similar to the affine-transformed average were then used to create an affine/deformable-transformed average. All original oriented stacks were then aligned to the affine/deformable-transformed average using affine and deformable transformation. The 24 registered stacks most similar to the affine/deformable-transformed average were then used to generate the final average acetylated tubulin reference template. The final average stack was unbiased, and was used for image registration.
Imaris was used for image processing (adjusting brightness and contrast uniformly) and to take virtual cross-sections of the VNC for comparison with siGOLD samples.

Morpholino injection

Morpholino injections were performed as previously described (Conzelmann et al., 2013a). We used the following morpholinos to target the various neuropeptide precursor genes (GeneTools, LLC): Pdu-FMRFa-start MO CCACTGGTCCCTCATGGCAGGGTTT, Pdu-PDF-start MO CTGAACTGTCTTGCTTGATCCCATC, Pdu-ATO-start MO CACAGGACTACCTTCATTTTTCTGA, Pdu-LUQ-start MO GTATTTGCACAACATAGTGATAGTC, Pdu-PENK-start MO GAGGAGGACCACCAATATCTTCATC, Pdu-RYa-start MO TATAGACATGACACCTTGTTGGAGT, Pdu-LEUC-start2 MO TCTTGGCTGAACTCATTGCGGCC, Pdu-FVa-start MO CCATCCGCCCACGCTCATATGCATC, Pdu-FVRIa-start MO CCCCCTTCATACTGTCACAACGGAC, Pdu-RGWa-start MO CGACGACCCCCTGTAGCTTCATGTC.

ACKNOWLEDGEMETS

We thank Matthias Flötenmeyer and Heinz Schwarz for advice on immunogold labeling and EM, Nadine Randel for help with tracing, Stephan Saalfeld for advice on the generation of an unbiased template for image registration, David Mastronarde for developing serialEM, Steffen Schmidt for maintaining our Catmaid server, Aurora Panzera for help with microinjections, and Dorothee Hildebrandt for animal care. The research leading to these results received funding from the European Research Council under the European Union's Seventh Framework Programme (FP7/2007-2013)/European Research Council Grant Agreement 260821. This project is supported by the Marie Curie ITN "Neptune", GA 317172, funded under the FP7, PEOPLE Work Programme of the European Commission.

REFERENCES

Asadulina, A., Panzera, A., Verasztó, C., Liebig, C. and Jékely, G. (2012). Whole-body gene expression pattern registration in Platynereis larvae. *Evodevo* **3**, 27.

Asadulina, A., Conzelmann, M., Williams, E. A., Panzera, A. and Jékely, G. (2015). Object-based representation and analysis of light and electron microscopic volume data using Blender. *BMC Bioinformatics* **16**, 229.

Backfisch, B., Veedin Rajan, V. B., Fischer, R. M., Lohs, C., Arboleda, E., Tessmar-Raible, K. and Raible, F. (2013). Stable transgenesis in the marine annelid Platynereis dumerilii sheds new light on photoreceptor evolution. *Proc Natl Acad Sci U S A* **110**, 193–198.

Bannister, S., Antonova, O., Polo, A., Lohs, C., Hallay, N., Valinciute, A., Raible, F. and Tessmar-Raible, K. (2014). TALENs mediate efficient and heritable mutation of endogenous genes in the marine annelid Platynereis dumerilii. *Genetics* **197**, 77–89.

Bargmann, C. I. (2012). Beyond the connectome: how neuromodulators shape neural circuits. *Bioessays* **34**, 458–465.

Bargmann, C. I. and Marder, E. (2013). From the connectome to brain function. *Nat Methods* **10**, 483–490.

Bauknecht, P. and Jékely, G. (2015). Large-Scale Combinatorial Deorphanization of Platynereis Neuropeptide GPCRs. *Cell Rep*.

Blumer, M. J., Gahleitner, P., Narzt, T., Handl, C. and Ruthensteiner, B. (2002). Ribbons of semithin sections: an advanced method with a new type of diamond knife. *J Neurosci Methods* **120**, 11–16.

Bock, D. D., Lee, W. C., Kerlin, A. M., Andermann, M. L., Hood, G., Wetzel, A. W., Yurgenson, S., Soucy, E. R., Kim, H. S. and Reid, R. C. (2011). Network anatomy and in vivo physiology of visual cortical neurons. *Nature* **471**, 177–182.

Briggman, K. L., Helmstaedter, M. and Denk, W. (2011). Wiring specificity in the direction-selectivity circuit of the retina. *Nature* **471**, 183–188.

Brorson, S. H. (1998). Comparison of the immunogold labeling of single light chains and whole immunoglobulins with anti-kappa on LR-white and epoxy sections. *Micron* **29**, 439–443.

Brorson, S. H. and Reinholt, F. P. (2008). The intensity of immunogold labeling of deplasticized acrylic sections compared to deplasticized epoxy sections-Theoretical deductions and experimental data. *Micron* **39**, 144–150.

Bucher, D. and Marder, E. (2013). SnapShot: Neuromodulation. *Cell* **155**, 482–482.e1.

Bumbarger, D. J., Riebesell, M., Rödelsperger, C. and Sommer, R. J. (2013). System-wide rewiring underlies behavioral differences in predatory and bacterial-feeding nematodes. *Cell* **152**, 109–119.

Cardona, A., Saalfeld, S., Preibisch, S., Schmid, B., Cheng, A., Pulokas, J., Tomancak, P. and Hartenstein, V. (2010). An integrated micro- and macroarchitectural analysis of the Drosophila brain by computer-assisted serial section electron microscopy. *PLoS Biol* **8**,.

Cardona, A., Saalfeld, S., Schindelin, J., Arganda-Carreras, I., Preibisch, S., Longair, M., Tomancak, P., Hartenstein, V. and Douglas, R. J. (2012). TrakEM2 software for neural circuit reconstruction. *PLoS ONE* **7**, e38011.

Collman, F., Buchanan, J., Phend, K. D., Micheva, K. D., Weinberg, R. J. and Smith, S. J. (2015). Mapping synapses by conjugate light-electron array tomography. *J Neurosci* **35**, 5792–5807.

Colombelli, J., Tängemo, C., Haselman, U., Antony, C., Stelzer, E. H., Pepperkok, R. and Reynaud, E. G. (2008). A correlative light and electron microscopy method based on laser micropatterning and etching. *Methods Mol Biol* **457**, 203–213.

Conzelmann, M. and Jékely, G. (2012). Antibodies against conserved amidated neuropeptide epitopes enrich the comparative neurobiology toolbox. *Evodevo* **3**, 23.

Conzelmann, M., Offenburger, S. L., Asadulina, A., Keller, T., Münch, T. A. and Jékely, G. (2011). Neuropeptides regulate swimming depth of Platynereis larvae. *Proc Natl Acad Sci U S A* **108**, E1174–E1183.

Conzelmann, M., Williams, E. A., Tunaru, S., Randel, N., Shahidi, R., Asadulina, A., Berger, J., Offermanns, S. and Jékely, G. (2013a). Conserved MIP receptor-ligand pair regulates Platynereis larval settlement. *Proc Natl Acad Sci U S A* **110**, 8224–8229.

Conzelmann, M., Williams, E. A., Krug, K., Franz-Wachtel, M., Macek, B. and Jékely, G. (2013b). The neuropeptide complement of the marine annelid Platynereis dumerilii. *BMC Genomics* **14**, 906.

De Paul, A., Mukdsi, J. H., Petiti, J. P., Gutierrez, S., Quintar, A. A., Maldonado, C. A. and Torres, A. I. (2012). Immunoelectron Microscopy: A Reliable Tool for the Analysis of Cellular Processes. In *Applications of Immunocytochemistry* (ed. Dehghani, H.), InTech.

Denk, W. and Horstmann, H. (2004). Serial block-face scanning electron microscopy to reconstruct three-dimensional tissue nanostructure. *PLoS Biol* **2**, e329.

Eipper, B. A., Stoffers, D. A. and Mains, R. E. (1992). The biosynthesis of neuropeptides: peptide alpha-amidation. *Annu Rev Neurosci* **15**, 57–85.

Gaudry, Q., Hong, E. J., Kain, J., de Bivort, B. L. and Wilson, R. I. (2013). Asymmetric neurotransmitter release enables rapid odour lateralization in Drosophila. *Nature* **493**, 424–428.

Gühmann, M., Jia, H., Randel, N., Verasztó, C., Bezares-Calderón, L. A., Michiels, N. K., Yokoyama, S. and Jékely, G. (2015). Spectral Tuning of Phototaxis by a Go-Opsin in the Rhabdomeric Eyes of Platynereis. *Curr Biol* **25**, 2265–2271.

Hamanaka, Y., Park, D., Yin, P., Annangudi, S. P., Edwards, T. N., Sweedler, J., Meinertzhagen, I. A. and Taghert, P. H. (2010). Transcriptional orchestration of the regulated secretory pathway in neurons by the bHLH protein DIMM. *Curr Biol* **20**, 9–18.

Hanaichi, T., Sato, T., Iwamoto, T., Malavasi-Yamashiro, J., Hoshino, M. and Mizuno, N. (1986). A Stable Lead by Modification of Sato Method. *Journal of Electron Microscopy* **35**, 304–306.

Hayworth, K. J., Morgan, J. L., Schalek, R., Berger, D. R., Hildebrand, D. G. and Lichtman, J. W. (2014). Imaging ATUM ultrathin section libraries with WaferMapper: a multi-scale approach to EM reconstruction of neural circuits. *Front Neural Circuits* **8**, 68.

Jékely, G. (2013). Global view of the evolution and diversity of metazoan neuropeptide signaling. *Proc Natl Acad Sci U S A* **110**, 8702–8707.

Jékely, G., Colombelli, J., Hausen, H., Guy, K., Stelzer, E., Nédélec, F. and Arendt, D. (2008). Mechanism of phototaxis in marine zooplankton. *Nature* **456**, 395–399.

Johard, H. A., Enell, L. E., Gustafsson, E., Trifilieff, P., Veenstra, J. A. and Nässel, D. R. (2008). Intrinsic neurons of Drosophila mushroom bodies express short neuropeptide F: relations to extrinsic neurons expressing different neurotransmitters. *J Comp Neurol* **507**, 1479–1496.

Koizumi, O., Wilson, J. D., Grimmelikhuijzen, C. J. and Westfall, J. A. (1989). Ultrastructural localization of RFamide-like peptides in neuronal dense-cored vesicles in the peduncle of Hydra. *J Exp Zool* **249**, 17–22.

Lin, T. Y., Luo, J., Shinomiya, K., Ting, C. Y., Lu, Z., Meinerzhagen, I. A. and Lee, C. H. (2015). Mapping chromatic pathways in the Drosophila visual system. *J Comp Neurol*.

Maco, B., Holtmaat, A., Cantoni, M., Kreshuk, A., Straehle, C. N., Hamprecht, F. A. and Knott, G. W. (2013). Correlative in vivo 2 photon and focused ion beam scanning electron microscopy of cortical neurons. *PLoS ONE* **8**, e57405.

Maco, B., Cantoni, M., Holtmaat, A., Kreshuk, A., Hamprecht, F. A. and Knott, G. W. (2014). Semiautomated correlative 3D electron microscopy of in vivo-imaged axons and dendrites. *Nat Protoc* **9**, 1354–1366.

Marder, E. (2012). Neuromodulation of neuronal circuits: back to the future. *Neuron* **76**, 1–11.

Martell, J. D., Deerinck, T. J., Sancak, Y., Poulos, T. L., Mootha, V. K., Sosinsky, G. E., Ellisman, M. H. and Ting, A. Y. (2012). Engineered ascorbate peroxidase as a genetically encoded reporter for electron microscopy. *Nat Biotechnol* **30**, 1143–1148.

Mastronarde, D. N. (2005). Automated electron microscope tomography using robust prediction of specimen movements. *J Struct Biol* **152**, 36–51.

Merighi, A., Cruz, F. and Coimbra, A. (1992). Immunocytochemical staining of neuropeptides in terminal arborization of primary afferent fibers anterogradely labeled and identified at light and electron microscopic levels. *J Neurosci Methods* **42**, 105–113.

Micheva, K. D. and Smith, S. J. (2007). Array tomography: a new tool for imaging the molecular architecture and ultrastructure of neural circuits. *Neuron* **55**, 25–36.

Mirabeau, O. and Joly, J. S. (2013). Molecular evolution of peptidergic signaling systems in bilaterians. *Proc Natl Acad Sci U S A* **110**, E2028–E2037.

Morgan, J. L. and Lichtman, J. W. (2013). Why not connectomics? *Nat Methods* **10**, 494–500.

Nässel, D. R. (1993). Insect myotropic peptides: differential distribution of locustatachykinin- and leucokinin-like immunoreactive neurons in the locust brain. *Cell Tissue Res* **274**, 27–40.

Ohyama, T., Schneider-Mizell, C. M., Fetter, R. D., Aleman, J. V., Franconville, R., Rivera-Alba, M., Mensh, B. D., Branson, K. M., Simpson, J. H., Truman, J. W., et al. (2015). A multilevel multimodal circuit enhances action selection in Drosophila. *Nature* **520**, 633–639.

Purschke, G. (1997). Ultrastructure of Nuchal Organs in Polychaetes (Annelida) - New Results and Review. *Acta Zoologica* **78**, 123–143.

Purschke, G. (2005). Sense organs in polychaetes (Annelida). *Hydrobiologia* **535**, 53–78.

Purschke, G., Wolfrath, F. and Westheide, W. (1997). Ultrastructure of the nuchal organ and cerebral organ in Onchnesoma squamatum (Sipuncula, Phascolionidae). *Zoomorphology* **117**, 23–31.

Randel, N., Asadulina, A., Bezares-Calderón, L. A., Verasztó, C., Williams, E. A., Conzelmann, M., Shahidi, R. and Jékely, G. (2014). Neuronal connectome of a sensory-motor circuit for visual navigation. *elife* **3**,.

Randel, N., Shahidi, R., Verasztó, C., Bezares-Calderón, L. A., Schmidt, S. and Jékely, G. (2015). Inter-individual stereotypy of the Platynereis larval visual connectome. *elife* **4**,.

Reyntjens, S. and Puers, R. (2001). A review of focused ion beam applications in microsystem technology. *J. Micromech. Microeng.* **11**, 287–300.

Rowley, J. and Moran, D. (1975). A simple procedure for mounting wrinkle-free sections on formvar-coated slot grids. *Ultramicroscopy* **1**, 151–155.

Saalfeld, S., Cardona, A., Hartenstein, V. and Tomancak, P. (2009). CATMAID: collaborative annotation toolkit for massive amounts of image data. *Bioinformatics* **25**, 1984–1986.

Schlötzer-Schrehardt, U. (1987). Ultrastructural investigation of the nuchal organs of Pygospio elegans (Polychaeta). *Zoomorphology*.

Schneider-Mizell, C. M., Gerhard, S., Longair, M., Kazimiers, T., Li, F., Zwart, M. F., Champion, A., Midgley, F., Fetter, R., Saalfeld, S., et al. (2015). Quantitative neuroanatomy for connectomics in Drosophila. *bioRxiv*.

Shu, X., Lev-Ram, V., Deerinck, T. J., Qi, Y., Ramko, E. B., Davidson, M. W., Jin, Y., Ellisman, M. H. and Tsien, R. Y. (2011). A genetically encoded tag for correlated light and electron microscopy of intact cells, tissues, and organisms. *PLoS Biol* **9**, e1001041.

Skepper, J. and Powell, J. (2008). Immunogold Staining of Epoxy Resin Sections for Transmission Electron Microscopy (TEM). *Cold Spring Harb Protoc* **2008**, pdb.prot5015–pdb.prot5015.

Stierhof, Y., Humbel, B. and Schwarz, H. (1991). Suitability of different silver enhancement methods applied to 1 nm colloidal gold particles: An immunoelectron microscopic study. *J Electron Microsc Tech* **17**, 336–343.

Timmermans, F. J. and Otto, C. (2015). Contributed Review: Review of integrated correlative light and electron microscopy. *Rev Sci Instrum* **86**, 011501.

Tomer, R., Denes, A. S., Tessmar-Raible, K. and Arendt, D. (2010). Profiling by image registration reveals common origin of annelid mushroom bodies and vertebrate pallium. *Cell* **142**, 800–809.

Tosches, M. A., Bucher, D., Vopalensky, P. and Arendt, D. (2014). Melatonin signaling controls circadian swimming behavior in marine zooplankton. *Cell* **159**, 46–57.

Urwyler, O., Izadifar, A., Dascenco, D., Petrovic, M., He, H., Ayaz, D., Kremer, A., Lippens, S., Baatsen, P., Guérin, C. J., et al. (2015). Investigating CNS synaptogenesis at single-synapse resolution by combining reverse genetics with correlative light and electron microscopy. *Development* **142**, 394–405.

Veedin-Rajan, V. B., Fischer, R. M., Raible, F. and Tessmar-Raible, K. (2013). Conditional and specific cell ablation in the marine annelid Platynereis dumerilii. *PLoS ONE* **8**, e75811.

Viswanathan, S., Williams, M. E., Bloss, E. B., Stasevich, T. J., Speer, C. M., Nern, A., Pfeiffer, B. D., Hooks, B. M., Li, W. P., English, B. P., et al. (2015). High-performance probes for light and electron microscopy. *Nat Methods* **12**, 568–576.

White, J. G., Southgate, E., Thomson, J. N. and Brenner, S. (1986). The structure of the nervous system of the nematode Caenorhabditis elegans. *Philos Trans R Soc Lond, B, Biol Sci* **314**, 1–340.

Williams, E. A., Conzelmann, M. and Jékely, G. (2015). Myoinhibitory peptide regulates feeding in the marine annelid Platynereis. *Front Zool* **12**, 1.

Wong, M. Y., Zhou, C., Shakiryanova, D., Lloyd, T. E., Deitcher, D. L. and Levitan, E. S. (2012). Neuropeptide delivery to synapses by long-range vesicle circulation and sporadic capture. *Cell* **148**, 1029–1038.

Yasuyama, K. and Meinertzhagen, I. A. (2010). Synaptic connections of PDF-immunoreactive lateral neurons projecting to the dorsal protocerebrum of Drosophila melanogaster. *J Comp Neurol* **518**, 292–304.

Zantke, J., Bannister, S., Rajan, V. B., Raible, F. and Tessmar-Raible, K. (2014). Genetic and genomic tools for the marine annelid Platynereis dumerilii. *Genetics* **197**, 19–31.

Zupanc, G. (1996). Peptidergic transmission: From morphological correlates to functional implications. *Micron* **27**, 35–91.

Figure titles and legends

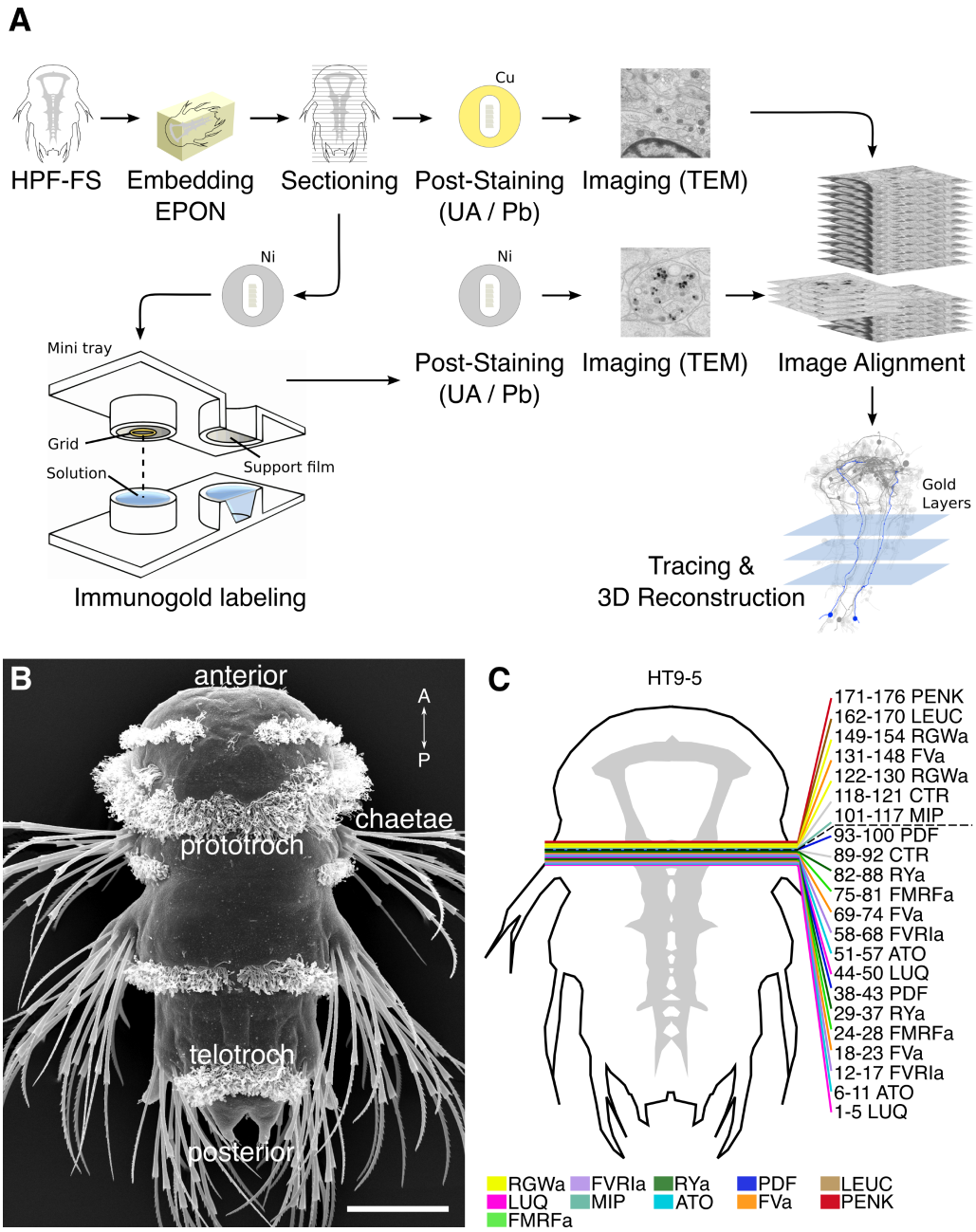

Figure 1. Development of the siGOLD method
(A) Schematic flowchart of the siGOLD labeling approach from high-pressure freezing and freeze substitution (HPF-FS) to tracing and 3D reconstruction. Ni, nickel grid, Cu, copper grid. (B) SEM micrograph of a 72 hpf *Platynereis* larva. (C) Schematic of the HT9-5 sample showing the position of the ventral nerve cord (VNC), ventral view. Colored lines indicate where cross-sections through the VNC were taken, near the base of the circumesophageal connectives at the level of the first commissure. Layer number(s) followed by neuropeptide ID are indicated for each colored line. Dashed line indicates the gap (approximately 10 missing sections) between the first and second series of sections. Scale bar: (B) 50 µm.

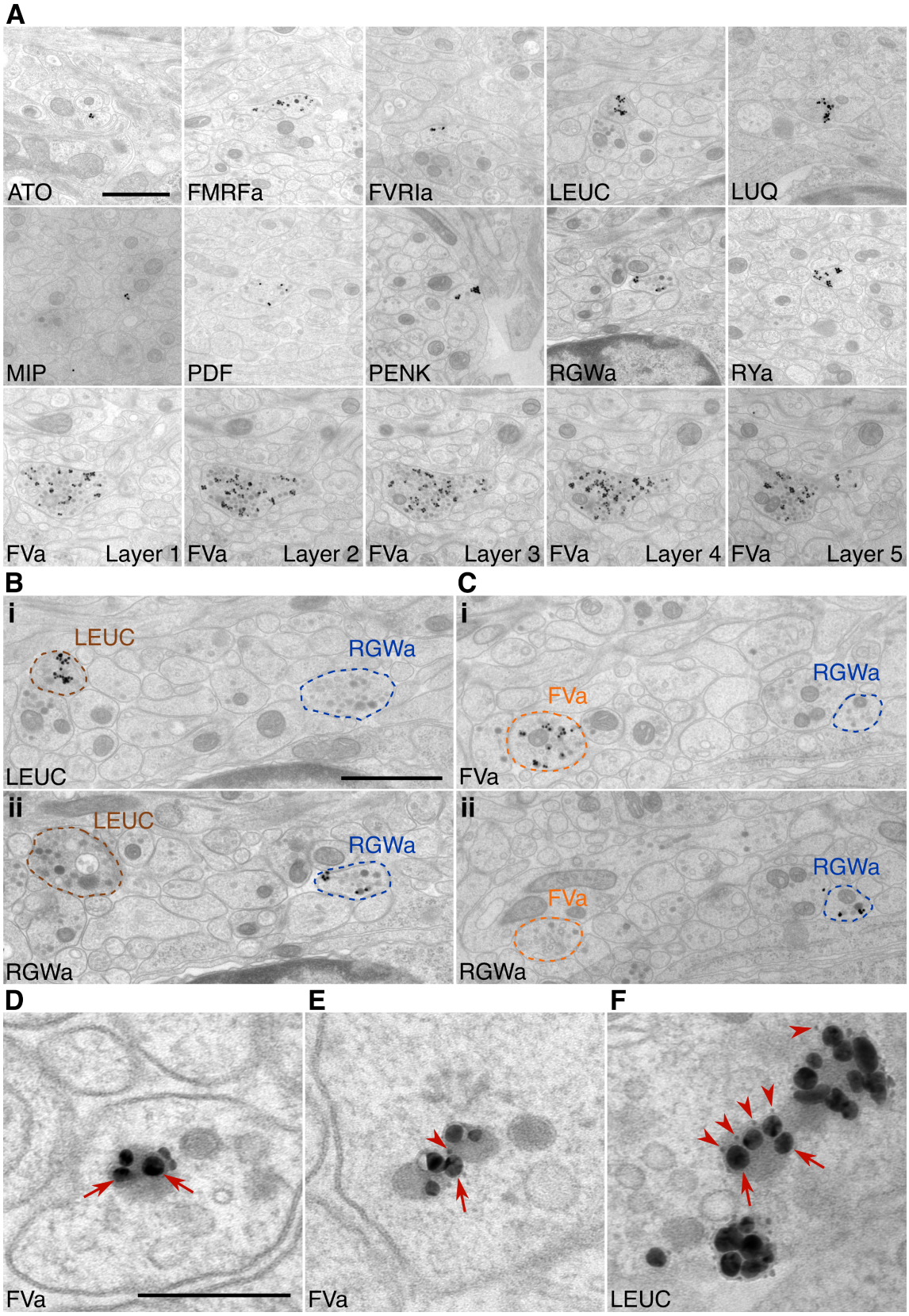

Figure 2. Labeling with siGOLD
(A) Representative micrographs with immunogold labeled axons for the neuropeptide antibodies indicated. For the FVa neuropeptide antibody, five adjacent sections are shown (FVa Layer 1-5). (B, C) Neurite-specific labeling in adjacent sections (7 sections apart) labeled with different antibodies. (D-F) High-resolution micrographs of immunogold labeled, silver-enhanced gold particles (arrows), and unenhanced ultra small gold particles (arrowheads) Scale bar: (A) 1 µm; (B-C) 200 nm; (D-F) 1 µm. High-resolution images are available in (Shahidi et al. 2015).

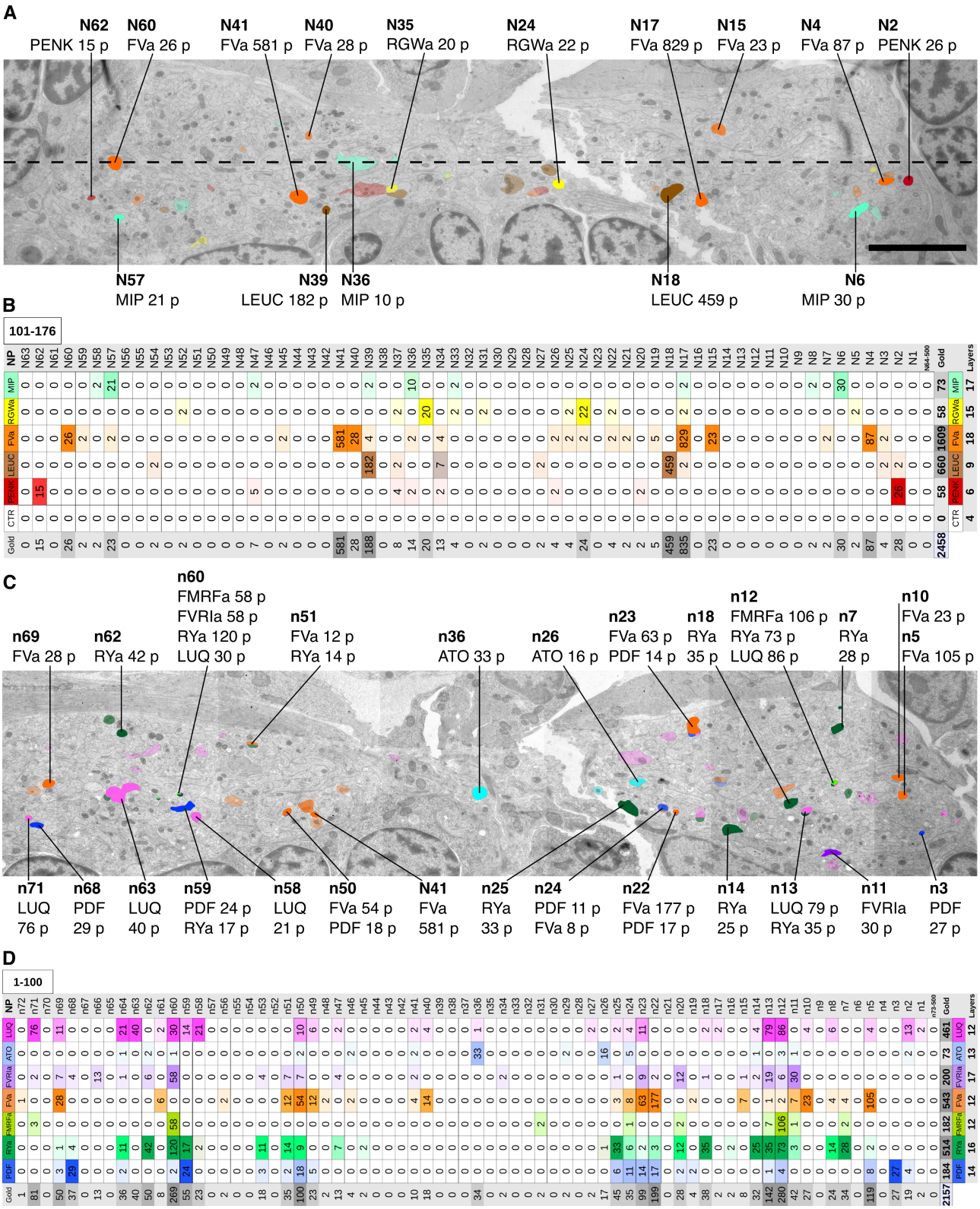

Figure 3. Identification of peptidergic neurites by siGOLD in a 72 hpf *Platynereis* specimen (A, C) Apical view of EM cross-section through the VNC near the first commissure. Dorsal side of larva is to the top. Strongly labeled neurites were analyzed across the whole VNC region. Control axon profiles were analyzed along a transect (dotted line), two axon profiles were sampled every 1 µm. Totals of 72 and 63 axons were examined for the first and second series of sections respectively (an approximately 10-section gap occurs between the two series). Colored cell profiles indicate gold labeled neuropeptidergic axons. Different shades of a color represent an approximation of labeling

intensity. Positive axons are tagged with neuron number, neuropeptide name, and total number of gold particles per total number of layers for that neuropeptide. (B, D) Tables show number of gold particles per axon for each neuropeptide. All strongly labeled axons across the VNC and control axons along the sampled transect are shown. Data were arranged according to the spatial distribution of the corresponding neurites in the VNC. Each sampled axon was traced across all layers and counted for its total number of gold particles. Columns indicate neurons and an ID with 'n' is given to each neuron in the first series of sections and 'N' for neurons in the second series of sections. Rows indicate neuropeptide immunogold labels. Different shades of the same color indicate intensity of gold labeling. Totals are shown for each row (neuropeptide) and each column (axon profile). In the final column of each table, the total number of layers stained for each neuropeptide is shown. Scale bar: 5 µm. Gold scores are available in Figure 3 – source data 1.

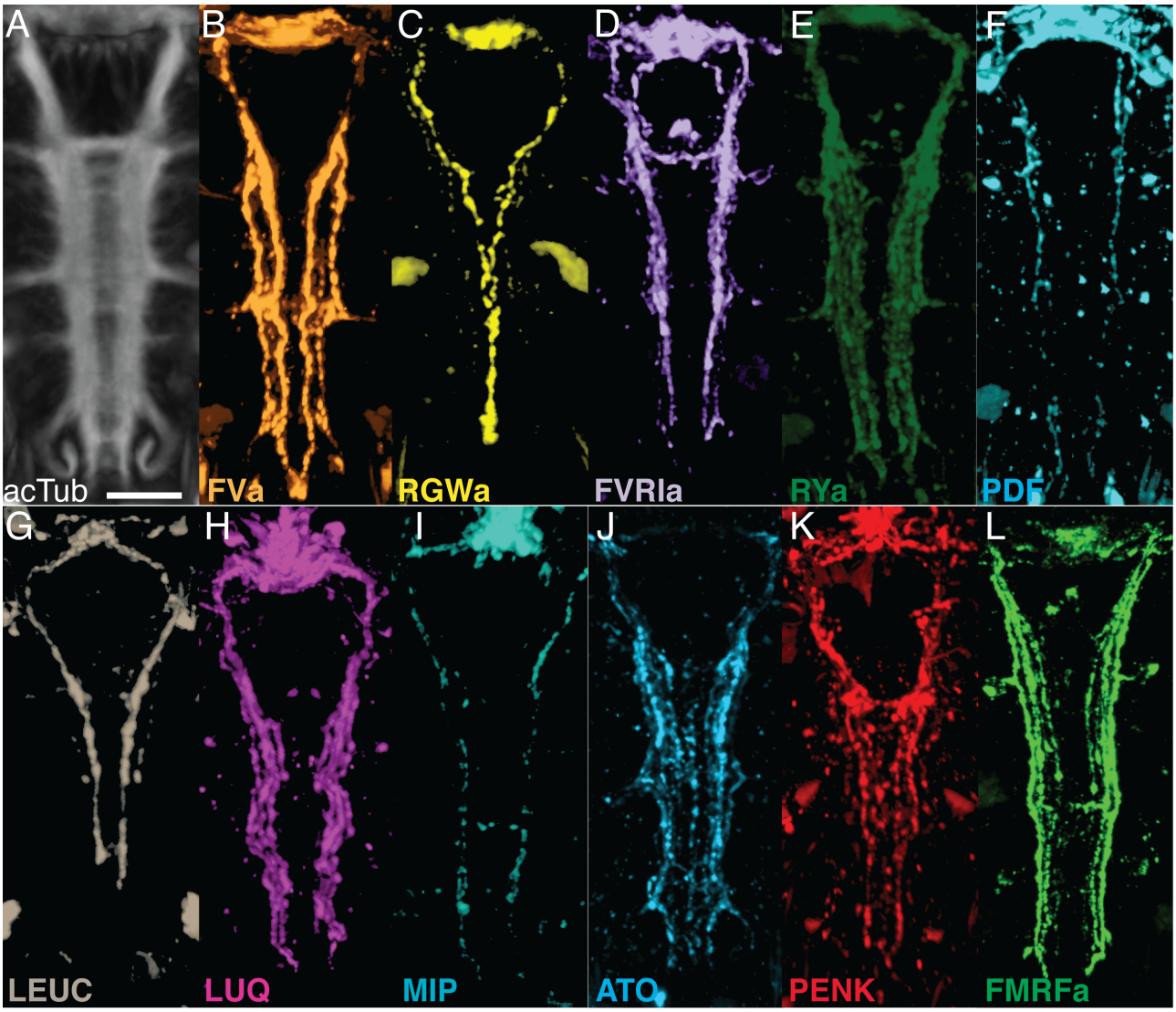

Figure 4. Whole-mount IF of *Platynereis* larvae with antibodies raised against neuropeptides labels distinct subsets of neuronal tracks in the VNC.
(A) Ventral view of *Platynereis* VNC, stained with an anti-acetylated tubulin antibody. This is the registered average VNC generated from scans of 36 larvae. (B-L) Whole-mount IF of *Platynereis* larvae with an antibody raised against (B) FVa, (C) RGWa, (D) FVRIa, (E) RYa, (F) PDF, (G) LEUC, (H) LUQ, (I) MIP, (J) ATO, (K) PENK, (L) FMRFa. Whole-mount scans were cropped to show only the VNC region. Scale bar: 20 µm.

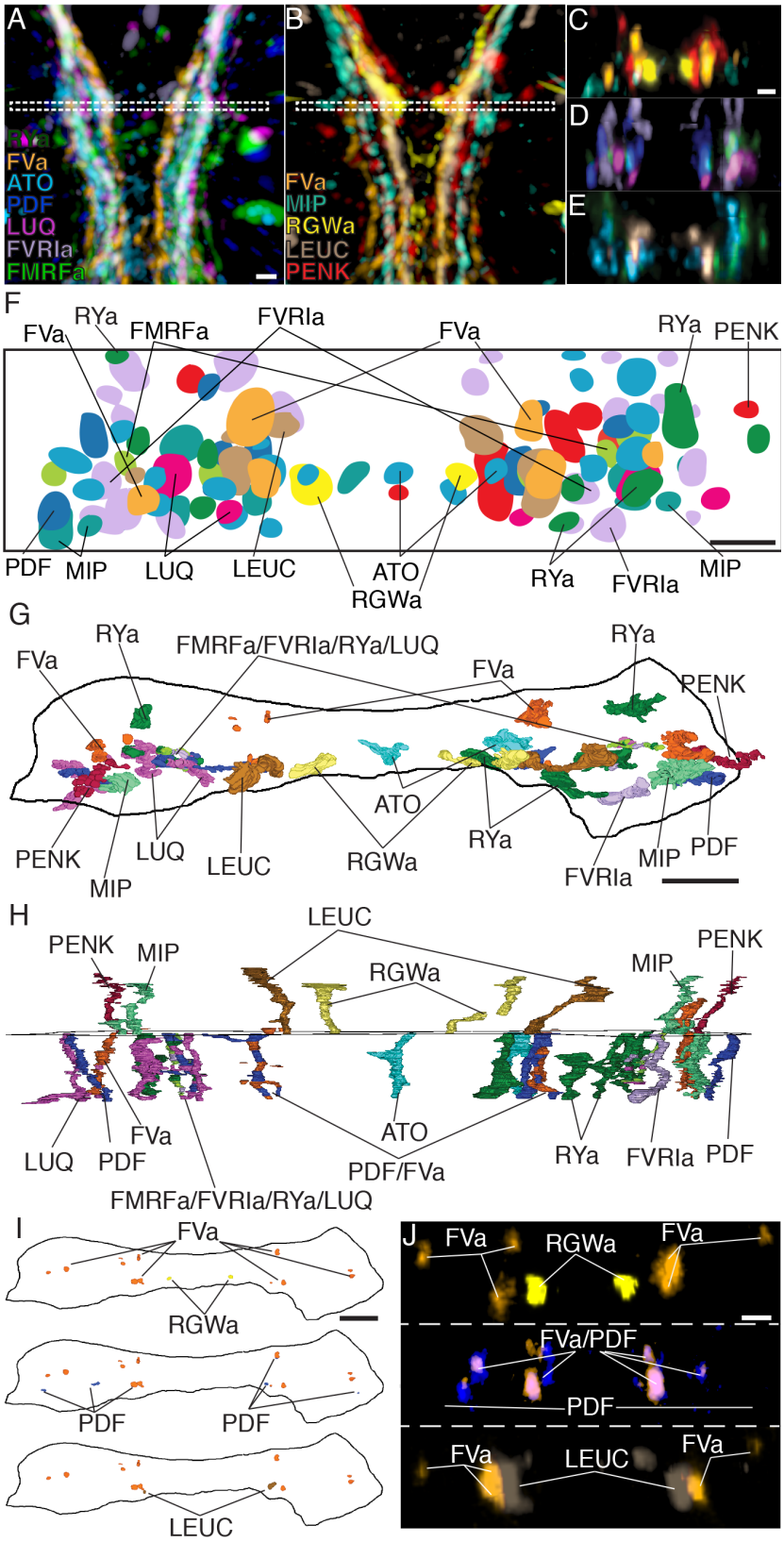

Figure 5. Axonal arrangements in the VNC detected by whole-body IF spatially match those detected by siGOLD.

(A, B) Ventral overview of individual registered full-body IF with antibodies raised against 11 different neuropeptides (colors). Image is cropped to show only the VNC in the first segment. White dashed box indicates the region where a 5 µm virtual transverse section shown in (C-E) was taken. (C-E) 5 µm virtual transverse section of individual registered full-body IFs from (A, B) in anterior

view to indicate their spatial position in the VNC relative to each other. (C) RGWa, FVa, PENK, MIP, (D) FVRIa, PDF, LUQ, FMRFa (E) RYa, LEUC, ATO. (F) Schematic overview of (C-E) indicating relative positioning of individual registered antibody stainings in the VNC, anterior view. (G, H) Reconstruction of neurites labeled by siGOLD in the VNC of specimen HT9-5 with antibodies raised against 11 different neuropeptides, (G) anterior view, (H) ventral view. For comparison with registered IF labeling in (A-F). (I) Position of neurites in specimen HT9-5 siGOLD-labeled with FVa and RGWa (top), FVa and PDF (middle), and FVa and LEUC antibodies (bottom). For comparison with double-IF in (J). (J) 2 µm virtual transverse sections of the VNC of 72 hpf *Platynereis* larvae double-stained with the FVa antibody (orange) and the RGWa (yellow, top), the PDF (blue, middle) or the LEUC (brown, bottom) antibodies. Scale bars: (A-E) 15 µm, (F - J) 5 µm.

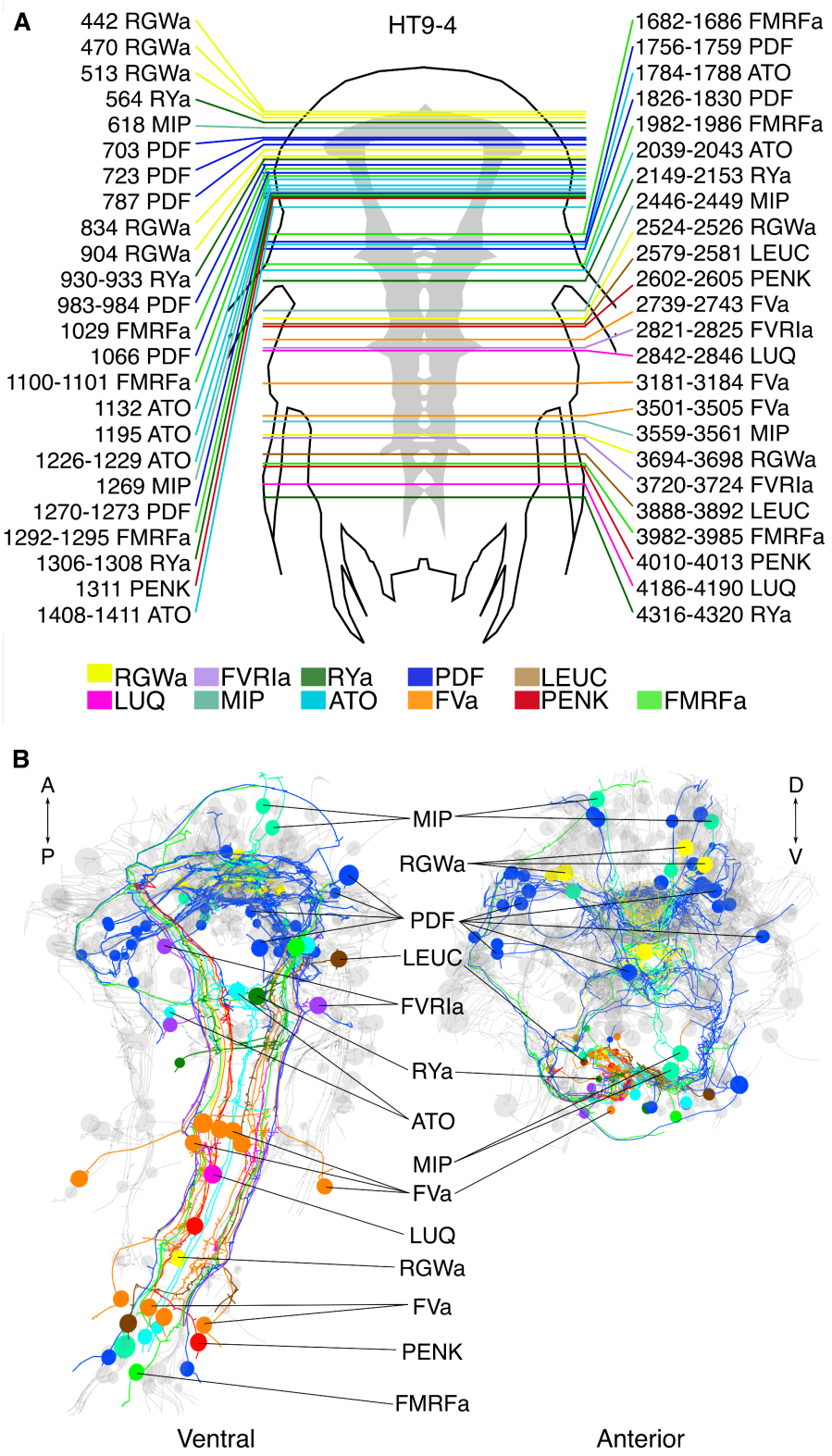

Figure 6. siGOLD labeling in a whole-body serial EM dataset
(A) Schematic of the HT9-4 specimen showing the position of the VNC (grey), ventral view. The entire larva was fully sectioned and imaged. Colored lines indicate the position of sections that were used for immunolabeling. For each line, layer number(s) followed by the name of the neuropeptide that was immunogold-labeled in those layers are indicated. (B) Ventral and anterior views of all fully traced immunogold-labeled peptidergic neurons. Detailed layer information is available in Figure 6 – source data 1.

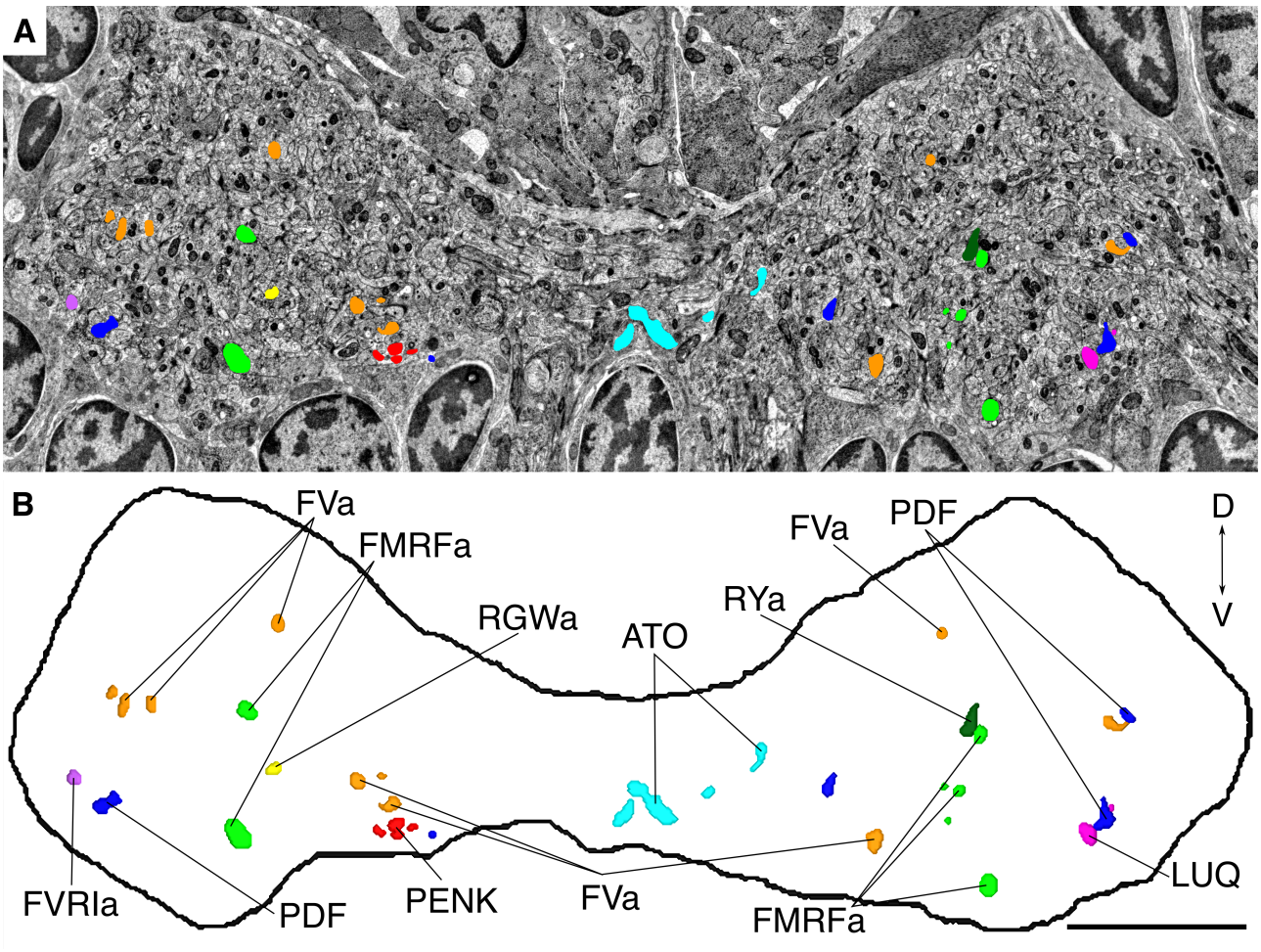

Figure 7. siGOLD labeling in the VNC cross-section
Micrograph (A) and segmented reconstruction (B) of a cross-section through the VNC near the base of the circumesophageal connectives at the first commissure showing the positions of all traced neuropeptidergic axons crossing the VNC at that level in the HT9-4 specimen. Scale bar: (B) 5 µm.

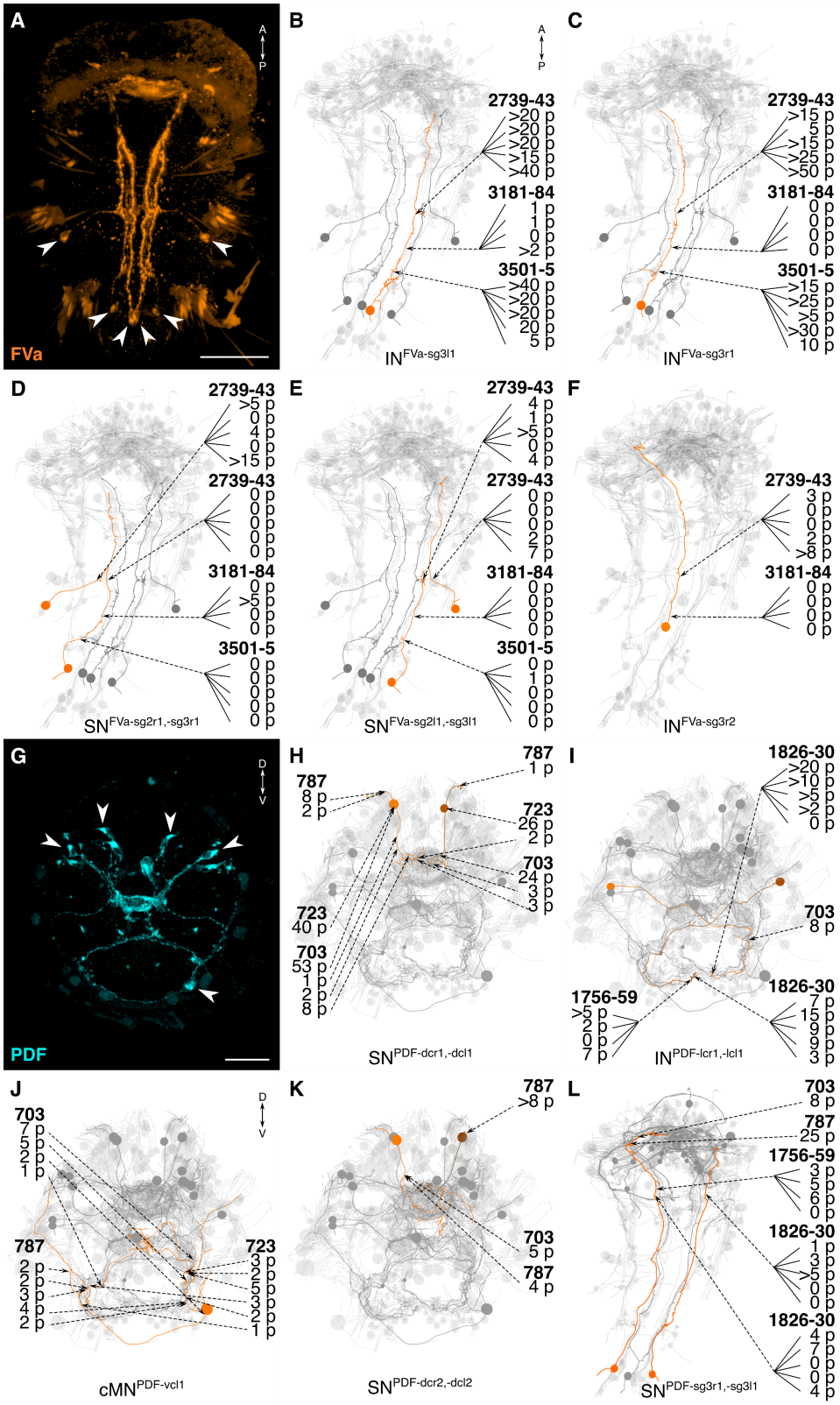

Figure 8. siGOLD labeling and whole-body neuron reconstructions
(A, G) Full body IF labeling of FVa and PDF positive cells, ventral view and anterior view, respectively. Note that (A) is 72 hpf and (G) is 48 hpf. Arrowheads point to neuron cell-bodies that were traced in EM reconstructions. (B-F, H-L) Fully reconstructed neurons, identified using the siGOLD method in the full body HT9-4 dataset. Dashed arrows indicate immunogold labeled layers along the neurite, layer number(s) and number of gold particles per layer are shown. Reconstructed FVa (B-F) and PDF (H-L) positive cells. Scale bars: (A) 50 µm; (G) 30 µm.

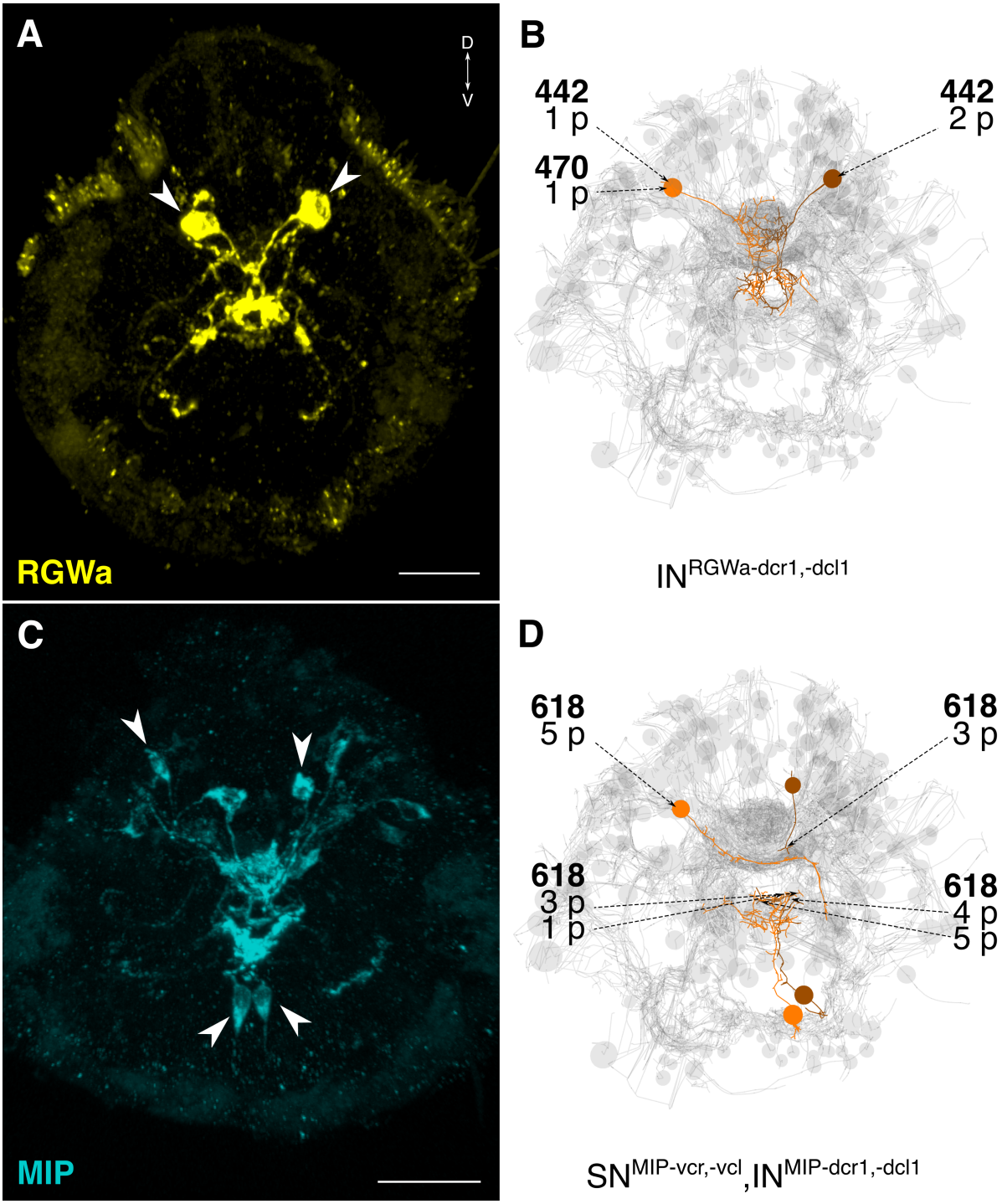

Figure 9. siGOLD labeling and whole-body neuron reconstructions
(A, C) Full body IF labeling of RGWa and MIP positive cells, in 72 hpf larvae, anterior views. Arrowheads point to neurons that were traced in EM reconstructions. (B, D) Traced neurons, identified using the siGOLD method in the full body HT9-4 dataset. Dashed arrows indicate immunogold labeled layers along the neurite, layer number(s) and number of gold particles per layer are shown. Reconstructed RGWa (B) and MIP (D) positive cells. Scale bars: (A, C) 30 µm.

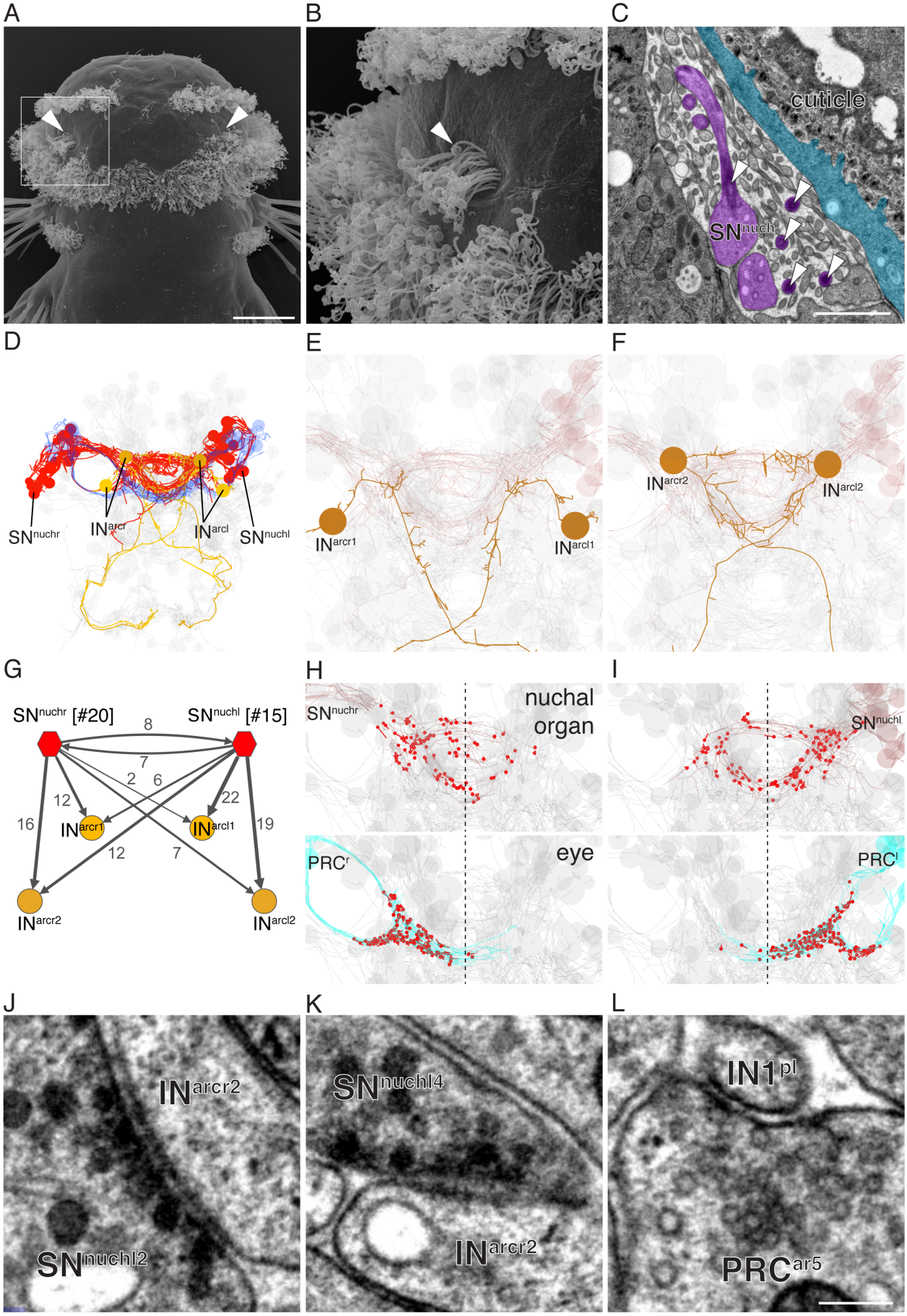

Figure 10. Reconstruction of a siGOLD-labeled peptidergic circuit
(A, B) SEM image of the nuchal organs (arrowhead) in the dorsal-posterior head of a 72 hpf *Platynereis* larva, dorsal view. Boxed area is shown enlarged in (B). Arrowheads point at motile

cilia above the olfactory pit. (C) TEM image of a cross section of the nuchal organ showing the olfactory pit with sensory neurons and microvilli. Arrowheads point at sensory cilia. Sensory endings in the olfactory pit are highlighted in magenta, an epithelial cell underneath the cuticle is highlighted in blue. (D) 3D reconstruction of the nuchal organ circuit. SN^{nuch} neurons (red), and IN^{arc} (orange) interneurons are shown. The photoreceptor cells of the adult eyes are shown in blue as a reference. (E, F) 3D reconstruction of IN^{arc} (orange) interneurons. (G) Graph representation of SN^{nuch} connectivity. Nodes represent neurons or groups of neurons, edges represent synaptic connections. The number of synapses is indicated on each arrow. Edge thickness is proportional to the number of synapses. (H, I) Presynaptic sites (red dots) in SN^{nuch} neurons and adult-eye photoreceptor cells (PRC) with their soma on the right (H) or left (I) side of the body. (J, K) Peptidergic synapses in SN^{nuch} neurons. (L) A glutamatergic synapse in an adult eye photoreceptor cell. Scale bar: (A) 30 µm; (C) 1 µm; (L) 150 nm.

Tables and titles

NP precursor name	**Abbreviation**	**Antigen**
FMRFamide	FMRFa	(C)FMRFa
RYamide	RYa	(C)VFRYa
Myoinhibitory peptide/ Allatostatin B	MIP	(C)AWNKNSMRVWa or (C)VWa
RGWamide	RGWa	(C)RGWa or (C)GWa
Proenkephalin	PENK	(C)YGDLSFSNSNYa
Luqin	LUQ	(C)WRPQGRFa
Allatotropin	ATO	(C)GFRTGAYDRFSHGFa
Pigment dispersing factor	PDF	(C)NPGTLDAVLDMPDLMSLa
leucokinin	LEUC	(C)KFTPWAa
FVamide	FVa	(C)AHRFVa or (C)FVa
FVRIamide	FVRIa	(C)FVRIa

Table 1. List of antibodies used
The full name and abbreviation of neuropeptide precursors that contain the neuropeptides used for immunoEM. The FMRFa, RYa, MIP short and long, RGWa, FVa short and long, and FVRIa antibodies have been described previously (Conzelmann and Jékely, 2012; Conzelmann et al., 2011; Conzelmann et al., 2013a; Jékely et al., 2008). All 11 neuropeptides are amidated (a). A Cys (C) was added to the N-terminus of each peptide to allow coupling during immunization and affinity purification. All antibodies were generated in rabbits. For FVa long, a rat antibody was also generated.

	layer				layer		
SN^{nuch}	703	723	787	**SN^{nuch}**	703	723	787
r1	0	2	0	**l1**	0	0	0
r2	0	0	0	**l2**	1	0	4
r3	0	0	0	**l3**	0	0	0
r4	0	0	7	**l4**	0	0	0
r5	0	0	0	**l5**	0	0	0
r6	2	0	0	**l6**	0	3	10
r7	0	0	0	**l7**	0	0	2
r8	0	1	2	**l8**	1	0	3
r9	0	0	0	**l9**	0	0	0
r10	0	0	0	**l10**	0	0	0
r11	0	0	0	**l11**	0	0	0
r12	0	3	0	**l12**	6	1	0
r13	1	3	2	**l13**	9	9	6
r14	0	0	0	**l14**	18	0	0
r15-r20	0	0	0	**l15**	0	0	0

Table 2. Number of gold particles in SN^{nuch} neurons in three layers labeled with the PDF antibody
Number of gold particles in SN^{nuch} neurons identified in three different immunogold layers labeled with the PDF antibody in all SN^{nuch} sensory neurons.

Additional files

Major dataset

The following dataset was generated:

Réza Shahidi et al. 2015.
High-resolution immunogold layers.
High-resolution images (2.22 nm/pixel) showing the area of the VNC. The archive contains one image file for each antibody.
http://dx.doi.org/10.5061/dryad.c7366

Supplementary files

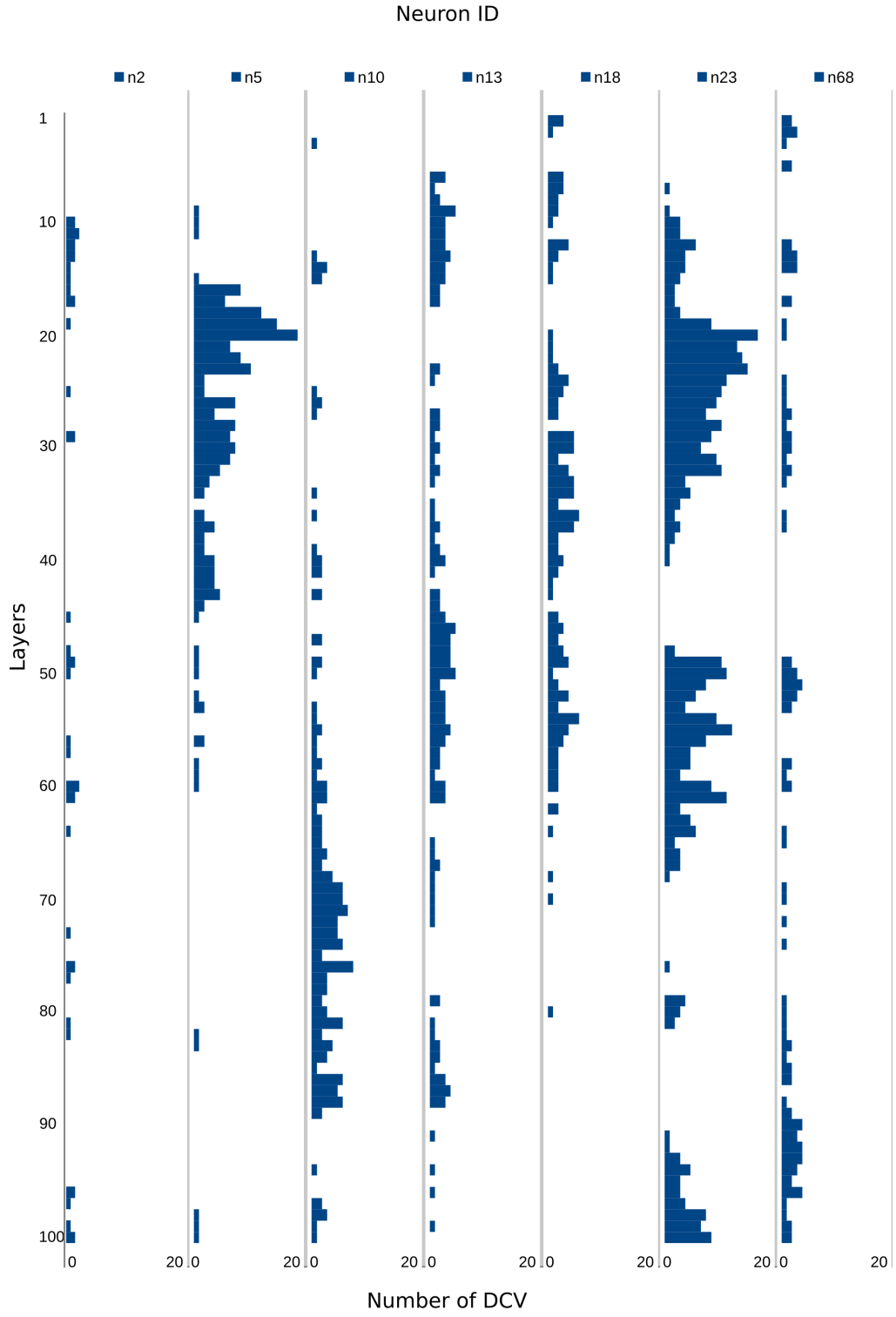

Figure 3 – figure supplement 1. Number of DCVs in selected neurite profiles along 100 layers. Number of DCVs scored along 100 layers in selected neurites in the HT9-5 dataset. The gold counts for the corresponding profiles are shown in Figure 3 – source data 1.

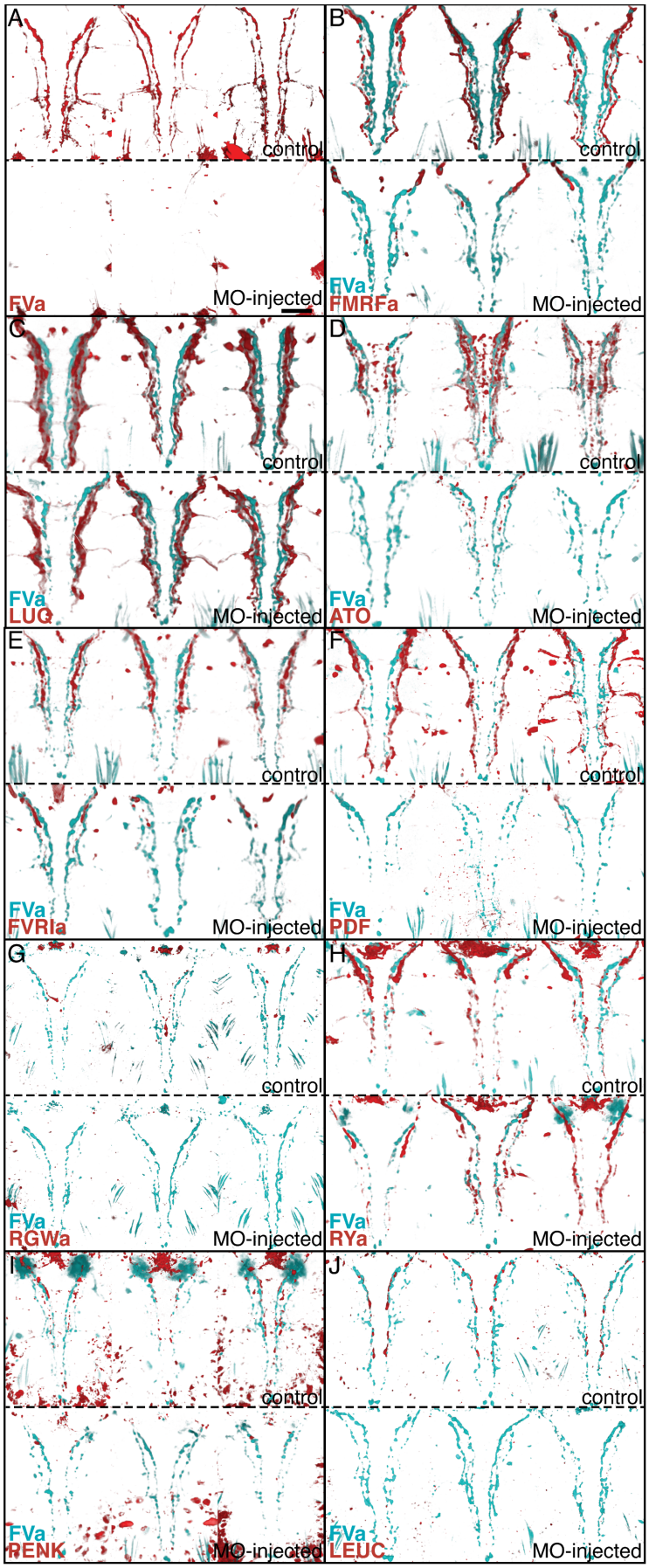

Figure 4 – figure supplement 1. Morpholino-mediated knockdown of proneuropeptides followed by whole-mount IF indicates antibody specificities.

Whole-mount IF of 72 hpf uninjected control *Platynereis* larvae and larvae micro-injected with translation-blocking morpholinos (MOs) targeting different neuropeptide precursor genes. FVa-knockdown and control larvae were stained with an antibody raised against FVa and counterstained with acetylated tubulin. All other control and knockdown larvae were co-stained with an antibody raised against FVa and an antibody raised against the MO target peptide indicated and counterstained with acetylated tubulin. All larvae are shown in ventral view. For each neuropeptide, three control larvae (top) and three MO-knockdown larvae (bottom) are shown. (A) FVa knockdown and control larvae with antibody raised against FVa. (B) FMRFa knockdown and control larvae with antibody raised against FMRFa. (C) LUQ knockdown and control larvae with antibody raised against LUQ. (D) ATO knockdown and control larvae with antibody raised against ATO. (E) FVRIa knockdown and control larvae with antibody raised against FVRIa. (F) PDF knockdown and control larvae with antibody raised against PDF. (G) RGWa knockdown and control larvae with antibody raised against RGWa. Note that the staining in the head is eliminated following knockdown. The staining in the VNC was too weak in these samples. (H) RYa knockdown and control larvae with antibody raised against RYa. (I) PENK knockdown and control larvae with antibody raised against PENK. (J) LEUC knockdown and control larvae with antibody raised against LEUC. Scale bar: 30 µm.

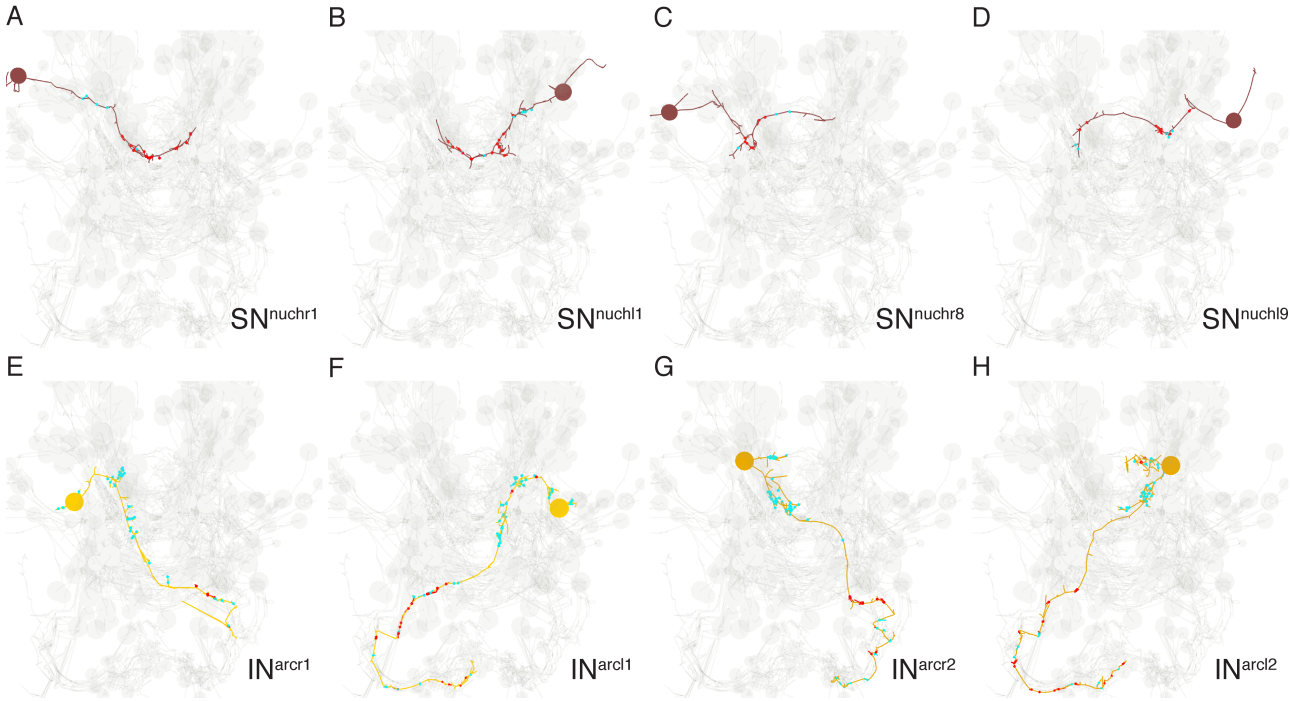

Figure 10 – figure supplement 1. Morphology of SN^{nuch} and IN^{arc} neurons.
(A, D) Four examples of SN^{nuch} sensory neurons with the presynaptic (red) and postsynaptic sites shown. (E, H) Morphology of the four IN^{arc} interneurons with the presynaptic (red) and postsynaptic sites shown.

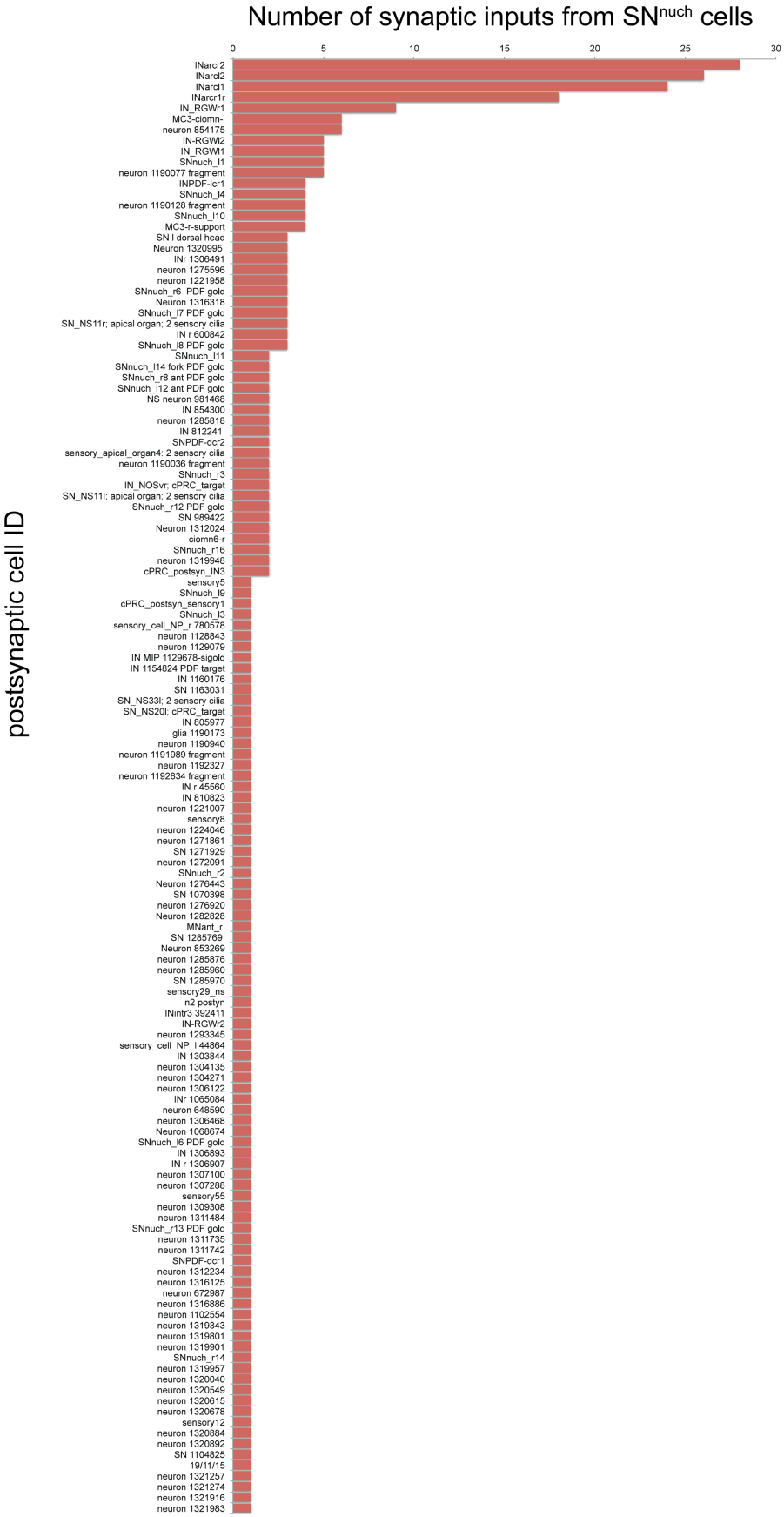

Figure 10 – figure supplement 2. Number of synaptic inputs from SN^{nuch} cells to all postsynaptic targets.

All postsynaptic targets of the SN^{nuch} neurons are listed.